

Award Accounts

The Chemical Society of Japan Award for Young Chemists for 2004

Molecular Assemblies of Functional Molecules on Gold Electrode Surfaces Studied by Electrochemical Scanning Tunneling Microscopy: Relationship between Function and Adlayer Structures

Soichiro Yoshimoto

National Institute of Advanced Industrial Science and Technology (AIST), Central 6, 1-1-1 Higashi, Tsukuba 305-8566

Received October 19, 2005; E-mail: so-yoshimoto@aist.go.jp

In this research, molecular assembly and function of aromatic thiols, porphyrins, phthalocyanines, and fullerenes on gold single crystal surfaces was studied by electrochemical methods and scanning tunneling microscopy (STM). Surface functions of promoter molecules such as pyridinethiols, pyrimidinethiols, and benzenethiol for cytochrome *c* electrochemistry were characterized by electrochemical techniques. Adlayer structures of those molecules were investigated by in situ STM, and molecular orientations for each molecule on the Au surfaces were clarified at molecular level. Adlayers of porphyrins and phthalocyanines for electrocatalytic reduction of dioxygen were examined to elucidate the relationship between activity and adlayer structure. Stable two-dimensional arrays of cobalt porphyrins indicated two-electron reduction of O_2 to H_2O_2, whereas two-step four-electron reduction of O_2 to H_2O occurred because of highly mobile porphyrinatoiron molecules on the surface. Furthermore, well-defined adlayers of crown-substituted phthalocyanine for host–guest interface and binary array consisting of porphyrin and phthalocyanine for the design of supramolecular nanoarchitectures were clearly visualized by STM. Finally, a unique approach for controlling molecular orientation was found by the formation of supramolecular assemblies consisting of porphyrin and fullerene. The electrochemical redox reaction of carbonyl and ferrocene moieties was promoted by using the simple method for the construction of a 1:1 supramolecular assembled film consisting of C_{60} derivative and octaethylporphyrinatometal on Au single crystal surfaces.

In the field of electrochemistry, surface modification is often used for controlling electron-transfer reactions and catalytic activity. Especially, the electron-transfer reaction of a metalloprotein is currently one of the most active areas in bioelectrochemistry and related fields.[1] Preparation of suitable interfaces to communicate with metalloproteins such as cytochrome *c*,[2,3] myoglobin,[4] and ferredoxin[5] is important for understanding biological functions of metalloproteins by conventional electrochemical techniques. On the other hand, the study of self-assembled monolayers (SAMs) of organothiols on metal substrates has been one of most active research fields in recent years.[6] SAMs have been extensively investigated in many fields including surface science,[6–8] photocatalysis,[9] electrochemistry,[10–12] lithography,[7b] and electronic devices.[6d,7b] Since early reports on SAMs, many functionally modified electrodes have been used to investigate the electrode reactions of metalloproteins.[2–5,13–16] Pyridinethiol (PySH) is one of the molecules used for earlier studies on SAMs.[2a] The PyS–SAMs such as 4-pyridinethiol (4-PySH) and di(4-pyridyl) disulfide (4,4′-PySSPy) have been well-known to be effective as so-called "electron-transfer promoters" for cytochrome *c* electrochemistry.[2] However, since many similar promoter molecules have been found to give more or less the same electrochemical response for cytochrome *c*,[2,3,15,16] the surface functions of the promoter molecules, i.e., the detailed interactions between cytochrome *c* and the surface modifier, have remained ambiguous. 2-Pyridinethiol (2-PySH) was also reported to be effective promoter molecule the same as 4-PySH for cytochrome *c*,[15] whereas another group reported that 2-PySH was much less effective than 4-PySH.[1a,15a] Such a discrepancy may partly come from the fact that the electrode surfaces so far used are not smooth on the atomic level. To obtain a much clearer answer to this problem, one should use atomically flat electrode surfaces, because the orientation of promoter molecule is strongly influenced by the situation of the underlying electrode surface.

Another attractive field is the electrochemistry of porphyrin thin films. Because porphyrins and related derivatives are included in metalloproteins as active centers, "hemes," it is necessary to understand their roles and electrochemical properties such as dioxygen storage.[17] After the late 1970's, thin films of porphyrinatometal and phthalocyaninatometal derivatives have been intensively studied due to the interest in electrocatalytic reactions, such as the reduction of O_2 for developing efficient fuel cells; such reactions occur mainly at graphite electrodes.[18–20] However, not much attention has been paid so far to the adlayer structure of those porphyrins; thus, the rela-

Published on the web August 7, 2006; doi:10.1246/bcsj.79.1167

tionship between the adlayer structure and the electrocatalytic activity is still unclear at the molecular level. Formation and characterization of ordered adlayers of porphyrin and phthalocyanine molecules at electrolyte–electrode interfaces are therefore important from the viewpoint of understanding the O_2 reduction mechanism.

Porphyrins also provide an extremely versatile synthetic base for a variety of material applications in many disciplines of chemistry and physics, such as opto-electronics, electrochemistry, catalysis, data storage, and solar cells.[21] Especially, covalently linked porphyrin–fullerene C_{60} dyads were found as one of artificial photosynthetic models in the mid 1990's.[22,23] It was also reported on non-covalent interaction between C_{60} and porphyrin cyclic dimer[24] and that between C_{60} and palladium-linked bisporphyrin.[25] Currently, porphyrin–fullerene supramolecular assemblies have been studied extensively to generate photocurrent as well as to elucidate their unique photophysical and photochemical properties.[26–30] Because fullerenes are known as one type of acceptors with the strong π-electron accepting ability, they are considered to be suitable building blocks for construction of three-dimensional molecular architectures. Supramolecular assemblies based on non-covalent interactions such as dipole–dipole,[31a] hydrogen bonding,[31b,32–37] and metal–ligand coordination[38,39] on metal surfaces, have been also explored in attempts to control surface properties.

In recent years, scanning tunneling microscopy (STM) has been widely accepted as a powerful tool for understanding the structure of adsorbed layers of molecules on metal surfaces at the atomic scale both in ultrahigh vacuum (UHV)[8,40,41] and in aqueous solution.[42–46] High-resolution STM has made it possible to directly determine packing arrangements and even internal structures of adsorbed organic molecules. It is demonstrated that in situ STM makes it possible to monitor, with atomic or molecular resolution, a wide variety of electrode processes such as the adsorption of water-soluble inorganic and organic species and underpotential deposition of metal ions.[42–46]

Nevertheless those molecules, especially, porphyrin and phthalocyanine derivatives, are very attractive for electrochemists, electrochemical investigations for those monolayers in aqueous solutions were difficult because of extreme low solubility for water. To overcome the difficulty, organic molecules were mainly dissolved in benzene and the modification onto the Au surface was carried out in benzene solution containing organic molecule in our research. The molecular assembly is significantly influenced by the kind of organic solvents, as reported by several groups,[47–49] although the choice of solvents can be tuned in function of the particular solute and/or substrate. On the other hand, adsorption of benzene on Au(111) surface is quite weak in our experimental condition, which encouraged us to investigate adlayers of water-insoluble organic molecules without interference of the adsorption of benzene. For example, we succeeded in forming a highly ordered (4×4) array of coronene on Au(111) for the first time.[50] This method is also effective for organic molecules that are easily decomposed by heating, for example, C_{60} dumbbell dimer, C_{120} molecule.[51] The evaporation technique used in UHV cannot be applied for the preparation of C_{120} adlayers, because it requires a relatively high temperature. Therefore, this method for the preparation of functional adlayers using benzene solutions is extendable to designs of highly ordered adlayers onto Au surfaces by using various functional organic molecules.

As mentioned above, to understand and to elucidate the nature of electrode surfaces and interfacial structures of modified surfaces at the electrochemical interface makes new designs of both modified-surface and supramolecular nanoarchitectures possible. In this article, molecular assemblies of functionalized molecules such as aromaticthiols, porphyrins, phthalocyanines, and fullerenes, both covalently and non-covalently bounded on Au electrode surfaces were focused, because those molecules have the possibility as building blocks for the construction of nanostructures. Electrochemical interfaces for (1) rapid electron-transfer reaction of cytochrome *c*, (2) O_2 reduction on porphyrin-modified surfaces, and (3) supramolecular assemblies consisting of porphyrin and fullerenes on Au single-crystal electrode surface were characterized by using electrochemical techniques and electrochemical STM. The relationships between adlayer structure and its surface function are described.

1. Preparation of Well-Defined Electrode Surfaces

As a fundamental basis for all STM studies, electrode–electrolyte interfaces must be prepared reproducibly, and methods must be established to observe these interfaces accurately. Well-defined single-crystal surfaces must be exposed to solution to understand surface structure–reactivity relationships on the atomic scale. It is still difficult to elucidate electrochemical reactions on the atomic scale using polycrystalline electrodes. Itaya's group succeeded in their efforts to produce extremely well-defined, atomically flat surfaces of various electrodes made of noble metals, base metals, and semiconductors without either oxidation or contamination in solution.[43]

A unique and very convenient way to prepare well-defined clean Pt surfaces for study in aqueous solutions was proposed by Clavilier et al. in 1980; in this procedure, mechanically prepared single-crystal electrode of Pt was annealed in an oxygen flame and quenched in pure water, the so-called "flame-annealing quenching method."[52] They also established a method of preparing a Pt single-crystal electrode by melting a Pt wire in the flame.[52] Such a technique was further extended for Au by Hamelin.[53] Since the report by Clavilier, studies of oxyanion adsorption have largely focused on the sulfate/hydrogensulfate ion, the most important representative of anions in the field of single-crystal electrochemistry. Especially, characteristic spikes, the so-called "butterfly" peak, were observed on Pt(111) electrode.[44,52] A similar voltammeric profile was found on Au(111) electrode by Conway and Hamelin's[53] and Kolb's groups.[54,55] It is now recognized as an order–disorder phase transition in the sulfate/hydrogensulfate adlayer. In particular, more detailed investigations were obtained via in situ STM.[44,46,56,57] Figure 1a shows typical cyclic voltammograms of an Au(111) single-crystal electrode prepared in our laboratory in 0.5 M H_2SO_4 recorded at a scan rate of $5\,mV\,s^{-1}$. Au oxidation was observed at 1.38 V, whereas the reduction of oxidized Au was occurred at 0.97 V. The red line indicates 50 times enlarged voltammogram in the double-layer region between -0.2 and 0.9 V. The voltammogram for the bare

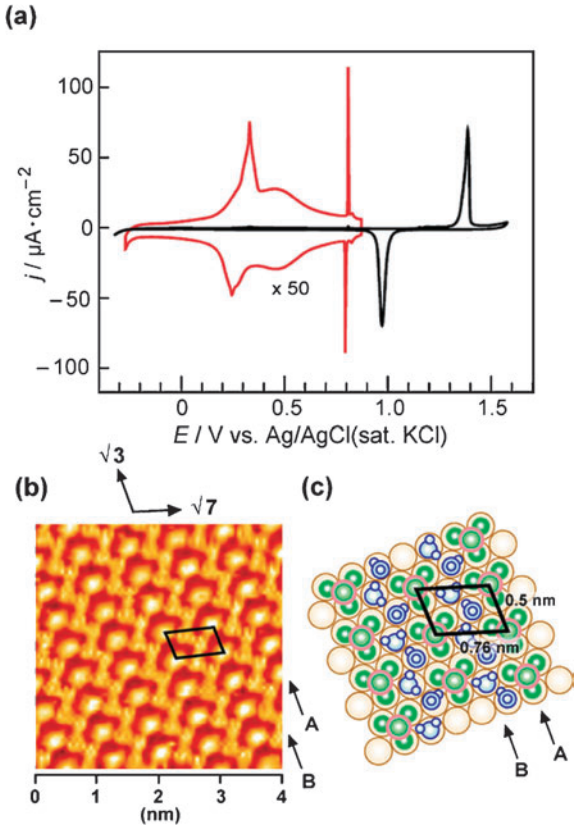

Fig. 1. (a) Typical cyclic voltammogram of a well-defined Au(111) electrode in a pure 0.5 M H_2SO_4 at scan rate of 5 mV s^{-1}. (b) In situ high-resolution STM image (4 × 4 nm^2) of ($\sqrt{3} \times \sqrt{7}$) sulfate/hydrogensulfate adlayer on Au(111) observed at 0.9 V versus Ag/AgCl and (c) corresponding proposed model.

Au(111) single-crystal electrode shown in Fig. 1a in the double-layer potential region (red line) is identical to that reported previously,[53d,55,57] indicating that a well-defined Au(111) surface is exposed to the solution. The anodic and broader peaks observed at 0.32 and 0.5 V are attributed to the anion-induced lifting of reconstruction, ($\sqrt{3} \times 22$) to (1 × 1) structure, and sulfate (or hydrogensulfate) adsorption, respectively. A pair of spikes observed at 0.8 V is due to the order–disorder phase transition of adsorbed sulfate/hydrogensulfate anions.[55–57] The order–disorder phase transition based on the CV profile is understood by in situ STM observation. Figure 1b shows a typical high-resolution STM image obtained at 0.9 V. A brightest spot marked by arrow A and two weaker spots marked by arrow B could be clearly seen in the high-resolution STM image. These bright rows are running along the [11$\bar{2}$], the so-called $\sqrt{3}$ direction, rotated by 30° with respect to the direction of the atomic rows of the underlying Au(111) lattice. The observed features on the Au(111) surface shown in Fig. 1b are very similar to those for the adsorbed sulfate/hydrogensulfate on Pt(111),[58] Rh(111),[59] Ir(111),[60] Pd(111),[61] and Cu(111).[62] One row consists of bright spots, whereas the other two rows consist of darker spots showing a zigzag feature between the bright rows. The high-resolution STM image revealed that there are clearly that two additional weaker spots between very bright ones.[63] As illustrated in Fig. 1c, the adlattice is assigned to be ($\sqrt{3} \times \sqrt{7}$) structure, which is identical to that obtained by several groups.[55–57]

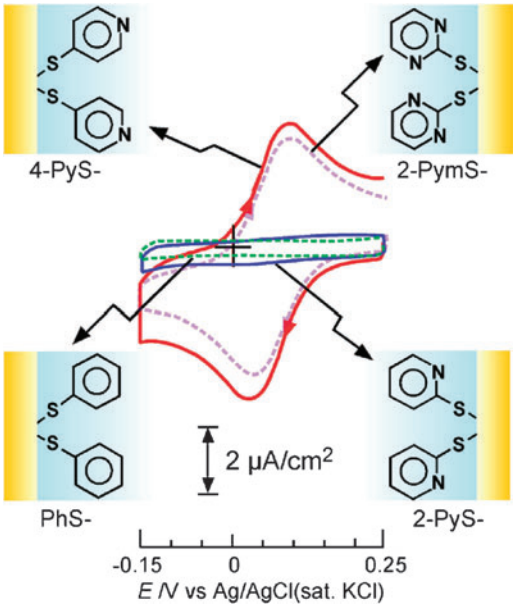

Fig. 2. Cyclic voltammograms of 100 μM horse heart cytochrome *c* in a phosphate buffer solution containing 0.1 M $NaClO_4$ (pH 7.0) at (a) 4-PyS- (red line), (b) 2-PyS- (blue line), (c) PhS- (green dotted line), and (d) 2-PymS- (purple dotted line) modified Au(111) electrodes. The scan rate was 50 mV s^{-1}.

2. Self-Assembled Monolayers on Gold

2.1 Surface Functionalities for Cytochrome *c* Electrochemistry. SAMs of promoter molecules on Au single-crystal surfaces have been studied to understand the mechanisms for electron-transfer reactions of metalloproteins. Especially, 4-PySH and 4,4′-PySSPy are often used as a promoter molecules for biological interfaces.[2,3b,3c] On the other hand, monolayers of 2-PySH, di(2-pyridyl) disulfide (2,2′-PySSPy) benzenethiol (PhSH) and diphenyldisulfide (PhSSPh) form self-assembled monolayers as well.[64] However, they do not possess such surface functionality so that they do not act as effective promoter molecules when atomically flat surfaces are used on the electrode.[65,66] The surface function still remains unclear yet for both the surface chemistry and metalloprotein electrochemistry.

As shown in Fig. 2, a 4-PyS-modified Au(111) electrode gave a well-defined voltammetric response of cytochrome *c*, whereas no electrochemical responses of cytochrome *c* were observed either at 2-PyS- or at PhS-modified Au(111) single-crystal electrode. The redox potential of cytochrome *c* was estimated to be 0.06 V vs Ag/AgCl (sat. KCl) from the anodic and cathodic potentials. The present results using Au(111) single-crystal electrodes obviously indicate that only the chemisorbed 4-PyS monolayer can promote a facile electron-transfer reaction between the Au(111) electrode and cytochrome *c* in solution,[66,67] as well as polycrystalline gold electrodes.[2] Because cytochrome *c* is basic metalloprotein (*p*I = ca. 10), especially, lysine residues ($-NH_3^+$) are positively charged in neutral solution.[13d,68] On the other hand, surface pK_a of 4-

PyS–Au was estimated to be 4.6 ± 0.5 by Crooks and Bryant.[69] Py moieties with the lone-pair are dominant due to the deprotonation in the 4-PyS–Au surface in neutral solution.[67b,70] It is considered that the 4-PyS–Au surface interacts electrostatically with positively charged lysine residues on the cytochrome *c* and plays a role in an inhibition of denaturized adsorption of cytochrome *c* onto electrode surface to promote properly electron-transfer reaction. Since many promoter molecules have been studied to realize the promoter activity on polycrystalline Au electrodes, several results have been also reported for 2-PyS-modified Au electrode.[1a,1c,64] Using well-defined Au(111) electrode, we found clear evidence that the 2-PyS-modified Au(111) electrode is not an active promoter at all for the electrochemical response of cytochrome *c*. Subsequently, we found that 2-pyrimidinethiol (2-PymSH) can also promote effectively the electron-transfer reaction of cytochrome *c*. From the CV profiles (purple dashed line) shown in Fig. 2, redox currents at 2-PymS-modified Au(111) electrode were found to be slightly smaller than that for 4-PyS-modifed Au(111) electrode. This is due to the difference in background current. An identical result was also observed when the corresponding disulfides (2,2′-PymSSPym) were used as a modifier. A 2-PymS-modified Au(111) electrodes gave a linear line between peak currents i_p and (scan rate)$^{1/2}$. Using a digital simulation technique,[1c] the redox potential, $E^{0\prime}$, the heterogeneous electron-transfer rate constant, $k^{0\prime}$, and the diffusion coefficient, D, were estimated to be 0.06 V vs Ag/AgCl (sat. KCl), 1.1×10^{-2} cm s^{-1} and 1.1×10^{-6} cm^2 s^{-1}, respectively, for horse heart cytochrome *c* at 20 °C. The surface functionality of promoter molecules for cytochrome *c* electrochemistry was clearly demonstrated by using Au single-crystal electrodes.

To understand the micro-orientation of such promoter molecules at electrochemical interfaces is important. In situ STM investigations were carried out in acidic aqueous solutions. As reported in our previous paper, because formation of SAMs from 4-PySH solution is strongly influenced by the presence of a small amount of impurities such as sulfide contained in commercially available 4-PySH, selection of modification condition is very important.[67] The modification was carried out for 20 μM 4-PySH aqueous solution for 10–20 min. Figure 3a shows a typical high-resolution STM image of a highly ordered 4-PyS monolayer acquired at 0.8 V vs RHE in 0.05 M $HClO_4$.[71] The ladder-like molecular rows consisting of the elliptic brightest spots aligned in [11$\bar{2}$] (the so-called $\sqrt{3}$) direction and located at the both sides of the ladder and slightly darker block spots in between, which correspond to the pyridyl (Py) units and thiolate S portions of the 4-PyS molecules, respectively. It is found in the STM result that a symmetrical arrangement of two chemisorbed 4-pyridinethiolates through the S positions can eventually be recognized as a repeating unit of the dimerized 4-PyS (i.e., a disulfide) for the ladder-like molecular rows.[66,71] On the basis of cross-sectional profiles, the intermolecular distances were measured to be 0.50 ± 0.02 and 1.45 ± 0.05 nm for $\sqrt{3}$ and [1$\bar{1}$0] atomic row directions, respectively. The rectangular unit cell is superimposed by white line in Fig. 3a as $p(5 \times \sqrt{3}R - 30^\circ)$ structure which is proper for the structure of 4-PyS monolayer. The proposed model is illustrated as a dimer state structure as shown in Fig. 3b. The $p(5 \times \sqrt{3}R - 30^\circ)$ unit cell yields a theoretical

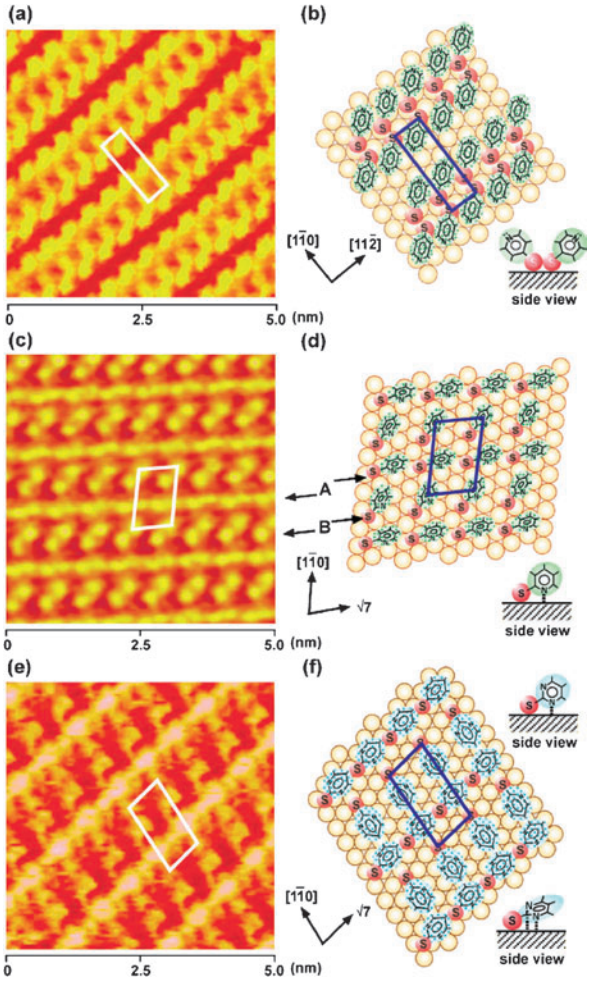

Fig. 3. Typical high-resolution STM images (5×5 nm^2) of (a) 4-PyS-, (c) 2-PyS-, and (e) 2-PymS-modified Au(111) in 0.05 M $HClO_4$ and (b, d, and f) corresponding proposed models. Reprinted with permission from Ref. 71 for STM image shown in (a), Copyright American Chemical Society (1998).

surface concentration of 4.6×10^{-10} mol cm^{-2}. According to a report by Porter et al., organothiolate can be electrochemically desorbed from Au surface in alkaline solution as in the following equation.[72]

$$\text{RS–Au} + \text{e}^- \rightarrow \text{RS}^- + \text{Au} \quad (1)$$

The electronic charge consumed by the reductive desorption of 4-PyS in 0.1 M KOH was calculated to be 44.4 μC cm^{-2} (4-PyS–Au + e$^-$ → 4-PyS$^-$ + Au), leading to the surface concentration of 4.6×10^{-10} mol cm^{-2},[66,67] therefore, it is consistent with that obtained from STM image.

Based on the STM image and the model, each 4-PyS possesses the molecular orientation with a nearly vertical molecular plane and a considerably tilted molecular axis of the pyridine ring with respect to the surface normal. The micro-orientation of the 4-PyS is probably essential for the rapid electron-transfer reaction of cytochrome *c*. Although 4-PyS molecules adsorb through S–Au bond formation and have the tilted molecular orientation of Py moiety as mentioned above, the N atom in each Py ring still faces the bulk solution. It is expected

that such micro-orientation of the pyridine rings will offer suitable sites for the electrochemical reaction: such sites allow cytochrome *c* to realize an appropriate interaction with the 4-PyS monolayer. Although investigations on PyS-SAMs on Au(111) using STM were subsequently reported by several groups, an identical adlayer structure of 4-PyS monolayer was found in each investigation.[73–76] However, a difference in adlayer structure between 4-PyS and 4,4′-PySSPy was found in 0.1 M H_2SO_4 by Kolb et al.[76] 4-PyS molecules formed both $(5 \times \sqrt{3})$ and $(10 \times \sqrt{3})$ structures on Au(111) at potentials more positive than 0.40 V (vs SCE), whereas the $(1 \times \sqrt{3})$ superstructure was found at 0.15 V. In the case of PySSPy-SAMs, a disordered structure was found at 0.65 V, while the $(7 \times \sqrt{3})$ structure was formed on Au(111) at 0.15 V. Kolb et al. explained tentatively that the $(1 \times \sqrt{3})$ superstructure was formed in 4-PyS-SAMs by coadsorption of sulfate/hydrogensulfate at negative potentials whereas such coadsorption did not take place on PySSPy-SAMs.[76] Although further investigations are needed, this is an interesting phenomenon for electrochemists.

The 2-pyridinethiolate (2-PyS) monolayer formed a completely different adlayer structure on Au(111).[67] The orientations of a 2-PyS monolayer were revealed by a high-resolution STM image, as shown in Fig. 3c. Two molecular rows with different orientation were running to the $\sqrt{7}$ direction. Although the STM image shown in Fig. 3c actually consists of many ordered spots, two molecular rows marked by arrows A and B are clearly seen on the terrace, both of which are parallel to a $\sqrt{7}$ direction. In the molecular row indicated by arrow A, the bright spots were aligned closely and the distance between the nearest spots was found to be 0.42 nm. If one takes the size of a 2-PyS molecule into consideration, the individual 2-PyS molecules are likely to be recognized as two spots, which probably originates from adsorption though S and N atoms of the 2-PyS with vertical orientation with respect to the Au surface. Note that the spots in arrow A are not aligned linearly, but are placed alternatively at slightly different positions, forming a zigzag arrangement. The direction of two spots corresponding to the vertically oriented 2-PyS is off by an angle of ca. 20° with respect to the $\sqrt{7}$ direction, suggesting the rotation of the molecular plane of pyridine rings. On the other hand, 2-PyS molecules in arrow B are rotated greatly, by an angle of about 50°, from the $\sqrt{7}$ direction. Although the 2-PyS appeared as two spots as well, the distance between the nearest spots in the molecular row indicated by arrow B is measured to be 0.46 nm in average, slightly wider than that in arrow A. These results indicate that the 2-PyS molecules in the molecular rows marked by arrows A and B sit in slightly different registries. The intermolecular spacings were found to be 0.75 ± 0.04 nm for $\sqrt{7}$ direction and 1.18 ± 0.05 nm for the $[1\bar{1}0]$ atomic row direction, corresponding to $\sqrt{7}$ and 4 times the Au lattice constant, respectively. According to our previous report, an adlayer structure of 2-PyS on Au(111) was assigned to have a $p(4 \times \sqrt{7}R - 40.9°)$ structure.[67] Taking the angle and direction of each molecular row with respect to the underlying Au lattice into consideration, we assigned the adlattice of the 2-PyS monolayer shown in Fig. 3c to have a $p(4 \times \sqrt{7}R - 19.1°)$ structure, which is a mirror image of $p(4 \times \sqrt{7}R - 40.9°)$. The 2-PyS monolayer on Au(111) was composed of several adlattices including mirror structures.[77] Note that other adlayer structures, $p(5 \times \sqrt{7}R - 19.1°)$ and $p(6 \times \sqrt{7}R - 19.1°)$, were also found on the terrace.[78] Such adlayer structures were affected by several factors such as concentration, solvent, temperature of modifying solution, and modification time.

We propose a structural model for the 2-PyS monolayer on Au(111) in Fig. 3d. A 0.76 nm × 1.15 nm parallelogram of the $p(4 \times \sqrt{7}R - 19.1°)$ unit cell was superimposed in Figs. 3c and 3d. In this model, it is assumed that the S atoms of the 2-PyS molecules sit at the bridge sites of Au(111) surface, because the 2-PyS molecule appeared as two spots with the short distances as described above. The 2-PyS molecules are positioned with two different rotation angles with respect to the $\sqrt{7}$ direction: One is 19.1° and the other is 49.1°. The former and latter correspond to the 2-PyS molecules in the arrows A and B in Fig. 3d, respectively. This model fits with STM observation and explains well the molecular arrangements of the 2-PyS monolayer on the Au(111) surface. As shown in Fig. 3c, two 2-PyS molecules in the $p(4 \times \sqrt{7}R - 19.1°)$ structure give a surface concentration of 3.8×10^{-10} mol cm^{-2}. This value is slightly smaller than the experimental value (4.7×10^{-10} mol cm^{-2}) of the surface concentration, which was obtained from CV of the reductive desorption for the 2-PyS-modified Au(111) electrode in 0.1 M KOH.[67] The difference in the values of surface concentration would be caused by the adsorption through S and N atoms of the 2-PyS molecules. Electrochemical desorption of 2-PyS molecules might involve two processes: the S–Au bond breaking and the desorption at the N atom of the Py group. Such reductive desorption should greatly affect the CV shape of the reductive desorption.[67] The micro-orientation of the 2-PyS molecules should not provide the activity for the cytochrome *c* electrochemistry. In the 2-PyS monolayer, the N atoms of the Py units are attached to the Au(111) surface, and do not face to the bulk solution. Such a micro-orientation cannot create active sites for the electrochemical reaction of cytochrome *c*. Adsorption of both thiolate S and pyridine N atoms of 2-PyS onto Au(111) electrode is also supported by the result for pH independency of the 2-PyS-modified Au surface using surface-enhanced IR absorption spectroscopy (SEIRAS).[70]

2-Pyrimidinethiolate (2-PymS) monolayer was prepared on Au(111) in the same manner. A typical high-resolution STM image is shown in Fig. 3e. The structure of the 2-PymS adlayer was very similar to that of the 2-PyS monolayer on Au(111). The adlayer was composed of two different parts aligning to the $\sqrt{7}$ direction, i.e., the brighter line part and a darker part consisting of two spots were alternately arranged.[70] Because corrugation heights between the two parts are different from each other (0.06 and 0.04 nm), we conclude that one orients perpendicular to the surface through thiolate S and pyrimidine N atoms in the brighter molecular row and the other takes an almost flat-lying orientation in the darker molecular row. From the cross-sectional profiles, the intermolecular spacings were found to be 0.75 ± 0.03 nm for $\sqrt{7}$ direction and 1.42 ± 0.05 nm for the $[1\bar{1}0]$ atomic row direction. The adlattice was determined to be $p(5 \times \sqrt{7}R - 19.1°)$ structure (leading to a surface concentration of 3.1×10^{-10} mol cm^{-2}). The structural model is proposed in Fig. 3f. In this model, the S atoms of

Table 1. CV Response of Cytochrome *c*, Surface Concentration, and Adlayer Structure for Each Molecule

Promoter molecule	Response of cytochrome *c*	Γ[a]/mol cm^{-2}	Adlayer structure[b]	Ref.
4-PyS (4,4′-PySS)	good	4.6×10^{-10}	$p(5 \times \sqrt{3}R - 30^\circ)$	66, 71
2-PyS (2,2′-PySS)	poor	4.7×10^{-10}	$p(4 \times \sqrt{7}R - 40.9^\circ)$[c]	66, 77
			$p(4 \times \sqrt{7}R - 19.1^\circ)$[c]	77
2-PymS (2,2′-PymSS)	good	5.1×10^{-10}	$p(5 \times \sqrt{7}R - 40.9^\circ)$[c]	70
			$p(5 \times \sqrt{7}R - 19.1^\circ)$[c]	78
2-PyzS	good	5.5×10^{-10}	$p(5 \times \sqrt{7}R - 19.1^\circ)$[c]	79
PhSH (PhSS)	poor	4.4×10^{-10}	partially ordered[d]	
MPA	good	6.8×10^{-10}	(3×3)	80
2-Amino-6-purinethiol	good	4.8×10^{-10}	0.76 nm × 0.77 nm rectangular[e]	81

a) Γ was calculated by electronic charge consumed by the reductive desorption in 0.1 M KOH. b) Adlayer structures were determined in 0.05 M $HClO_4$. c) Predominant structure. Other structures were also seen. d) It was obtained in our modification condition. e) STM imaging was carried out in 0.06 M $NaClO_4$ solution (pH 6.6).

2-PymS molecules sit on the bridge sites of the Au(111) lattice. The pyrimidine moieties orient with two different tilt angles, i.e., one pyrimidine N atom attaches perpendicularly to the Au surface and two pyrimidine N atoms interact with the Au surface (flat-lying orientation), as depicted with side views. These models would be enough to explain why the rapid electron-transfer reaction of cytochrome *c* is possible, because pyrimidine N atoms always face to the bulk solution. Note that another structure, $p(4 \times \sqrt{7}R - 19.1^\circ)$, was also found in highly ordered 2-PymS monolayer on Au(111).[78] Surface functions of modified electrodes for the rapid electron transfer of cytochrome *c* were further examined by using new surface modifiers. Au(111) electrodes modified with 2-pyrazinethiol (2-PyzSH), an isomer of 2-PymSH, gave an excellent voltammetric response of cytochrome *c*.[79] The STM images of 2-PyzS-modified Au(111) surfaces were similar to that of either 2-PyS- or 2-PymS-modified Au(111), suggesting that 2-PyzSH adsorbed at both thiolate S and pyrazine N atoms, with the pyrazine ring being perpendicular to the electrode surface. The 2-PyzS-modified surface has another pyrazine N atom faced to the solution, through which cytochrome *c* can interact. The pyridine, pyrimidine, and pyrazine N atoms faced to the solution are key factors for the rapid electron transfer of cytochrome *c* on these modified electrodes. SAMs of 2-amino-6-purinethiol[16] and carboxy-terminated alkanethiols[7] such as 3-mercaptopropionic acid (MPA), which is also well-known as an effective promoter for cytochrome *c* electrochemistry, were investigated on Au(111) by in situ STM observation.[80,81]

In the case of a PhS monolayer on Au(111), only disordered structure was obtained. Sometimes, ordered domains were partially seen on the Au(111) terraces. The intermolecular distance between bright spots in ordered molecular arrays was approximately 0.5 nm (not shown). On the basis of the reductive desorption in 0.1 M KOH, the electronic charge was calculated to be 42.5 μC cm^{-2}, leading to a surface concentration of 4.4×10^{-10} mol cm^{-2}.[66] The result suggests that the adlayer structure of a PhS monolayer is similar to those of the 4-PyS- and 2-PyS-modified Au(111). Wan et al. subsequently reported that $(\sqrt{13} \times \sqrt{13})R13.9^\circ$ symmetry of PhS monolayer was formed on Au(111).[82] According to their report, the ordered phase was formed within a few minutes in 0.1 mM PhSH aqueous solution and multilayers were obtained by further immersion of the substrate. Although further investigations are needed, PhS-modified Au(111) electrode prepared in our condition cannot communicate with cytochrome *c* because of the hydrophobicity of the electrode surface. Various values for each promoter molecule are summarized in Table 1.

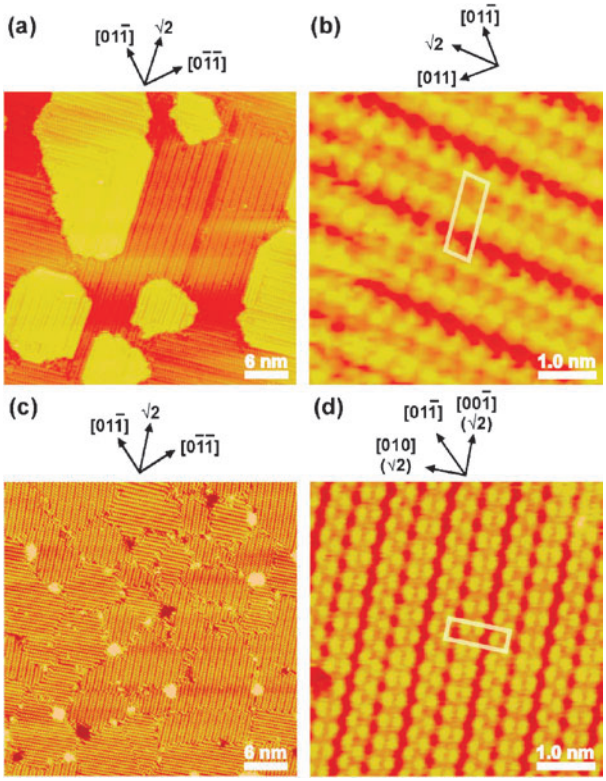

Fig. 4. Typical large-scale (40×40 nm^2) and high-resolution (5×5 nm^2) STM images of (a and b) 4-PyS- and (c and d) 2-PyS-modified Au(100)–(1×1) surface observed in 0.05 M $HClO_4$. Reprinted with permission from Ref. 83 for panels (a) and (b), Copyright Elsevier Science (2000).

These molecules also formed highly ordered molecular layers on Au substrate with a different crystallographic orientation. For example, on the Au(100)–(1×1) surface with square lattice, each terrace was completely covered with a highly ordered 4-PyS monolayer as shown in Figs. 4a and 4b.[83] Some islands were also observed on the atomically flat terrace. The height of the island on the (100)–(1×1) terrace was ca.

0.24 nm, which corresponds to the Au monoatomic height. The molecular rows of 4-PyS monolayer align to [010], the so-called $\sqrt{2}$ direction. Careful inspection revealed that step lines of each Au islands aligned to either atomic row or $\sqrt{2}$ direction, suggesting that Au islands diffuse during the adsorption process of 4-PyS. No molecular defects with monoatomic pits were observed on the terrace, although such defects usually appear during the self-assembling process of either 4-PySH or 4,4′-PySSPy on the Au(111) surface in 0.05 M $HClO_4$. Both 4-PySH and 4,4′-PySSPy molecules formed a highly ordered $p(\sqrt{2}R45^\circ \times 5R53.1^\circ)$ structure with disulfide formation. The intermolecular distances of 0.41 ± 0.02 nm for the $\sqrt{2}$ direction and 1.43 ± 0.05 nm for the other direction of the unit cell were obtained in a 0.05 M $HClO_4$ solution. The main difference in structure for the adsorbed 4-PySH was found in the $p(\sqrt{2}R45^\circ \times 5R53.1^\circ)$ structure on the Au(100)–(1 × 1) surface and the $p(5 \times \sqrt{3}R - 30^\circ)$ structure on the Au(111) surface, where a more densely packed ($\sqrt{3}/\sqrt{2}$ times) structure for adsorbed 4-PySH on Au(100) surface was seen than that on the Au(111) surface. The surface excess was calculated to be $(5.8 \pm 0.2) \times 10^{-10}$ mol cm^{-2} from the electronic charge consumed by the reductive desorption of 4-PyS: Such a result is consistent with that calculated (5.7×10^{-10} mol cm^{-2}) on the basis of the $p(\sqrt{2}R45^\circ \times 5R53.1^\circ)$ unit cell. The 4-PyS monolayer chemisorbed on a Au(100)–(1 × 1) single-crystal electrode was effective for the rapid electron-transfer reaction of cytochrome *c*.[65,83] On the other hand, typical STM images of 2-PyS monolayer formed on Au(100)–(1 × 1) surface are shown in Figs. 4c and 4d. The adlayer structure of 2-PyS was completely different from that of 4-PyS. Highly ordered arrays with two rotational domains are observed clearly with some small etching pits at domain boundaries, as shown in Fig. 4c. The rows of domain cross each other at the angle of 90° because of the 2-fold symmetry of the Au(100)–(1 × 1) structure. For 2-PySH (or 2,2′-PySSPy) modification onto Au(100)–(1 × 1) surface, the formation of etching pits was found in a few cases, but the size of each etching pit was much smaller than that of 4-PyS monolayer on Au(111) surface. In the high-resolution STM image shown in Fig. 4d, the individual 2-PyS molecules were clearly seen in the molecular rows as two bright spots. Careful inspection revealed the presence of molecular rows consisting of a set of two bright spots with two different molecular orientations alternately aligned to the $[00\bar{1}]$ direction. The intermolecular spacings were found to be 0.41 ± 0.02 nm for $[00\bar{1}]$ direction and 1.21 ± 0.03 nm for [010] direction, corresponding to $\sqrt{2}$ and $3\sqrt{2}$ times the Au lattice constant, respectively, whereas the distance between nearest spots was approximately 0.31 nm. The unit cell was superimposed as a $(\sqrt{2} \times 3\sqrt{2})R45^\circ$ structure in Fig. 4d.[84] As reported in our previous paper,[66] because 2-PyS-modified Au(100)–(1 × 1) electrode did not indicate any electrochemical response of cytochrome *c*, it is consistent that each 2-PyS molecule in highly ordered domains adsorbs through S and N atoms of 2-PyS perpendicular to the Au(100) surface, the same as the case on Au(111).

2.2 Surface Design for Host–Guest Interface. Calixarene derivatives, which are cyclic oligomers, have been well-known to form complexes with specific metal ions and organic guest molecules in the host–guest and stereo-selective chemistry.[85,86] Recently, to prepare functionalized electrodes for molecular recognition, those compounds have been immobilized on metal surfaces through the formation of SAMs.[87–91] Analytical and electrochemical applications have been developed for the host–guest recognition using calixarene derivatives.[87,88] However, details of sensing interfaces are still unclear in electrolyte solutions, because those studies were carried out with polycrystalline metal electrodes. STM and atomic force microscopy (AFM) investigations of adlayers of calix[4]arene[89a] and resorcin[4]arene[89b,90] derivatives containing long alkyl chain thiols or sulfide moieties on Au surfaces have been reported in ambient atmosphere[89] and UHV environment.[90] In an electrolyte solution, the formation of a self-organized array of calix[4]arene on Au(111) was reported by Kunitake's[91] and Wan's groups.[92] The calix[4]arene molecule was found to form a dimer structure, i.e., the two molecules in a cone conformation with sideway orientation are connected to each other in a "head-to-head" orientation through the OH groups. To design highly ordered functional surfaces for host–guest molecular recognition, we synthesized *p-t*-butylcalix[4]arene-1,3-dithiol (BCAD), which has a flattened cone conformation with two thiol moieties (see Fig. 5a).[93]

We first attempted to modify a freshly annealed Au(100) substrate by immersion into an ethanol solution of ca. 100 μM BCAD. In general, adsorption of organothiols onto Au surfaces is performed by simple immersion of the substrate into an ethanol solution containing organothiols for more than

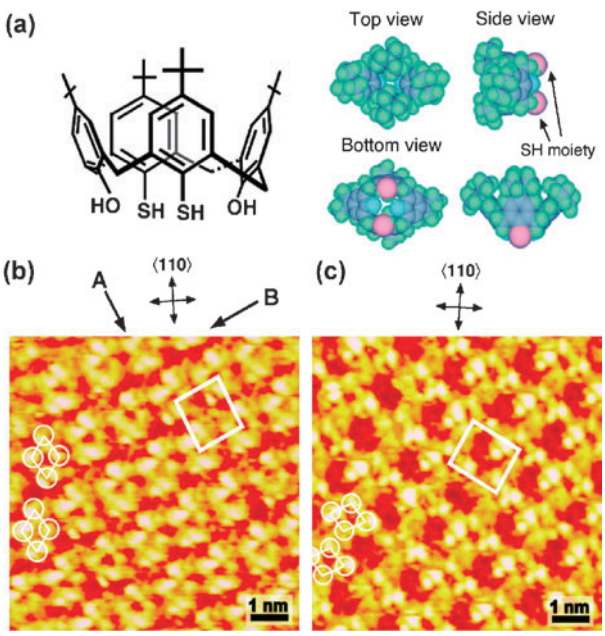

Fig. 5. (a) Illustration of chemical structure and space filling model of *p-t*-butylcalix[4]arene-1,3-dithiol (BCAD). (b) and (c) High-resolution STM images of highly ordered BCAD adlayer on Au(100)–(1 × 1) in 0.05 M $HClO_4$. Potentials of the substrate and the tip were held at 0.85 and 0.35 V, respectively. The tunneling current was 2.0 nA. The two arrow signs indicate close-packed directions of the Au(100)–(1 × 1) substrate. Reprinted with permission from Ref. 95, Copyright American Chemical Society (2003).

12 h.[9,10] However, when the modification was carried out in this manner, we could not obtain clear STM images of individual BCAD molecules. The STM image of the BCAD-modified Au(100) surface in 0.05 M $HClO_4$ revealed rough surface features, indicating the formation of multi-layers. This is considered to be due to the strong interaction between BCAD molecules. Therefore, to control the adlayer structure and molecular orientation, we carried out the modification more carefully by injecting an aqueous solution saturated with BCAD molecules into 0.05 M $HClO_4$. The high-resolution STM images revealed the symmetry and internal molecular structure of BCAD in the ordered domain. Two different packing arrangements of BCAD molecules were found on the Au(100)–(1×1) surface, as shown in Figs. 5b and 5c. Each molecule is seen in the shape of a rhombus, as marked by four white circles in the STM image. The four bright spots seem to correspond to *p*-*t*-butyl units. The distances between the two diagonal centers of the bright spots are measured to be 0.71 ± 0.03 and 1.18 ± 0.06 nm, respectively: these results can be compared with those estimated from the molecular model and agree within the experimental error. The size of the observed BCAD molecule on the Au(100)–(1×1) surface is in good agreement with that derived from the crystal structure of BCAD.[94] The set of four bright spots indicated by white circles in Fig. 5b is attributable to four *t*-butyl groups in one BCAD molecule (upper-rim), suggesting that each BCAD molecule is oriented perpendicularly to the surface through two thiol moieties of lower-rim. The arrow A shows the $\sqrt{5}$ direction with respect to the Au lattice direction. On the basis of the cross-sectional profiles, intermolecular spacings of BCAD indicated by arrows A and B were measured to be 1.28 ± 0.05 and 1.57 ± 0.05 nm, respectively, which correspond to $2\sqrt{5}$ and $\sqrt{29}$ times the Au lattice constant. The unit cell is superimposed in Fig. 5b. On the basis of the STM image described above, we tentatively assigned the unit cell defined in Fig. 5b to the $p(2\sqrt{5}R26.7^\circ \times \sqrt{29}R21.8^\circ)$ structure, which leads to a surface concentration of 8.0×10^{-11} mol cm^{-2}. The adlattice shown in Fig. 5c is identical to the $p(2\sqrt{5}R26.7^\circ \times \sqrt{29}R21.8^\circ)$ structure, but the packing arrangement is different from that shown in Fig. 5b.[95]

It is noteworthy that no highly ordered adlayer of BCAD was seen on the terrace when Au(111) was used as the substrate. The preliminary result suggests that the structure of chemisorbed BCAD layer depends upon the crystallographic orientation of Au. Such a dependency was also found for bis(9,10-dioxo-2-anthryl) disulfide-modified Au(111) and Au(100)–(1×1) surfaces.[96] Thus, the suitable selections of solvent, substrate, and potential are important for precise control of molecular orientation of complicated compounds like calixarene.[95]

3. Molecular Assemblies of Porphyrin and Phthalocyanine

3.1 Electrochemical Reduction of Molecular Oxygen. Thin films of metalloporphyrins and their derivatives have been intensively studied because of the interest in electrocatalytic reactions, such as the reduction of O_2, mainly at graphite electrodes.[18–20,97,98] For example, Anson and Shigehara reported a two-step 4-electron reduction of O_2 on graphite electrodes with adlayers of porphyrinatocobalt(II) (CoP),[20a] 2,3,7,8,12,13,17,18-octaethylporphyrinatocobalt(II) (CoOEP),[20] and other cobalt porphyrins.[20d] However, as mentioned in the introduction, the relationship between adlayers and electrochemical activity is not still clear because a multilayer of porphyrins was formed at a rough electrode surface.

Adlayer structures of porphyrins and phthalocyanines derivates were studied in the past, mostly in UHV using STM on various metal surfaces.[31,99–104] STM has also been used to understand the structure of adlayers of water-soluble porphyrin molecules in solution.[105–110] Highly ordered arrays of 5,10,15,-20-tetrakis(*N*-methylpyridinium-4-yl)porphyrin (H_2TMPyP) molecules were formed on the I–Au(111),[105] I–Ag(111),[106] I–Pt(100),[107] and S-modified Au(111)[108] electrodes. However, the ordering of porphyrin array directly attached on a bare Au(111) surface at electrochemical interface was subsequently reported by He et al.[109] Potential modulation plays a significant role for controlling the surface mobility of tetra(4-pyridyl)porphyrin (TPyP) molecules.[109] Tao and co-workers also investigated the adlayers of three water-soluble molecules, protoporphyrinatoiron(III), protoporphyrinatozinc(II), and protoporphyrin(IX), on the graphite basal plane in aqueous solutions with both STM[110a,110b] and AFM.[110a]

We subsequently investigated several water-insoluble porphyrin adlayers such as CoP,[111a] CoOEP,[111a] tetraphenylporphyrinatocobalt(II) (CoTPP),[111b] and phthalocyaninatocobalt(II) (CoPc)[111c] and we succeeded in forming highly ordered molecular arrays of those molecules spontaneously on Au(111) surfaces by immersing Au(111) in benzene solutions containing those molecules. High-resolution STM images for each molecular adlayer are shown in Fig. 6. In the case of CoP, although each CoP molecule can be discriminated, few ordered domains are seen. When the potential was kept at 0.75 V, a slightly more negative potential than the OCP, highly ordered domains of CoP were formed. The intermolecular distance was found to be 1.18 ± 0.05 nm, 4 times the atomic distance on Au(111)–(1×1). Therefore, the ordered adlayer structure obtained at 0.75 V was assigned to (4×4). The closely packed (4×4) structure of CoP was steadily observed in the potential range between 0 and 0.75 V. When the potential was returned to a value more positive than 0.8 V, the highly ordered (4×4) structure was again changed into a disordered structure.[111a] For the other adlayers such as CoOEP, CoTPP, and CoPc molecules, stable and highly ordered arrays were formed on the Au(111) surface. The adlayers were not dependent upon electrode potential until near the H_2 evolution potential in $HClO_4$. The adlayer structures of CoOEP and CoTPP formed in benzene solutions were identical to those obtained in UHV.[103] The CoOEP and CoTPP adlayers formed an incommensurate structure with respect to the reconstructed Au(111) surface; hence, the exact relation between the CoOEP adlayer and the underlying Au(111) lattice could not be determined. CoOEP and CoTPP layers fully cover the Au(111) surface, whereas CoP allows open spaces to remain on Au(111); for CoOEP and CoTPP, a larger interaction between the molecules and a smaller interaction between the molecules and the surface might be expected, compared with the corresponding interactions for CoP.

In the case of CoPc, high-resolution STM images also revealed the characteristic shape, internal structure, and orientation of each CoPc molecule in ordered domains. CoPc mole-

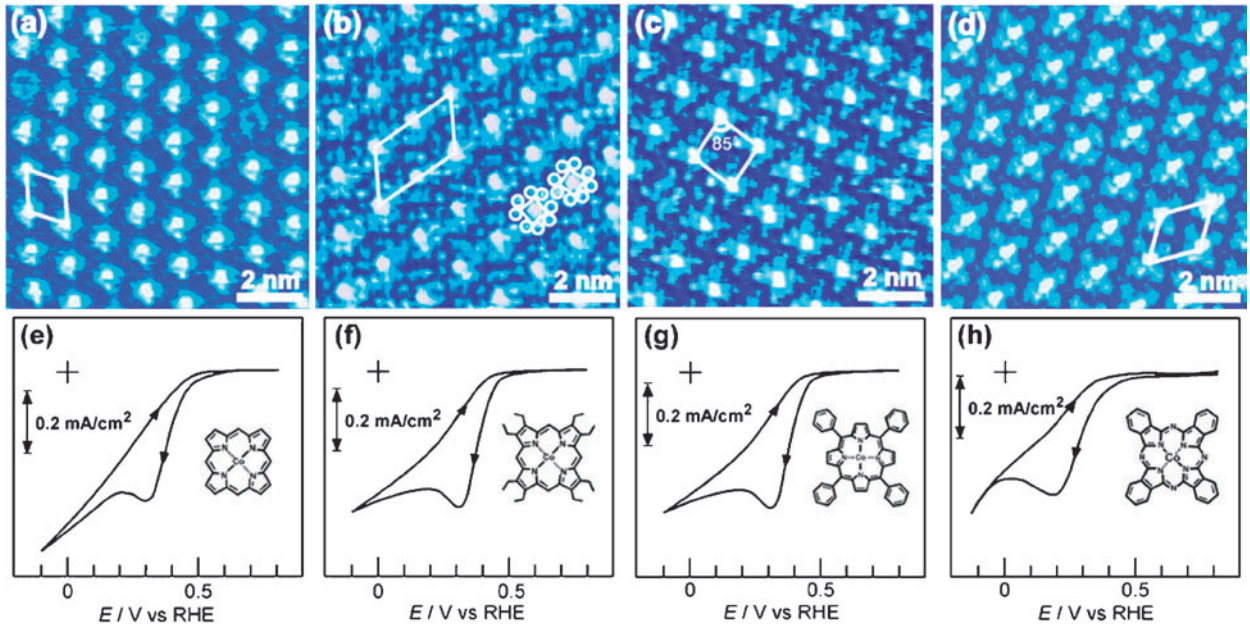

Fig. 6. High-resolution STM images ($9 \times 9\,nm^2$) of (a) CoP, (b) CoOEP, (c) CoTPP, and (d) CoPc adlayer on Au(111) in 0.1 M $HClO_4$ acquired at 0.75 V for (a) and 0.85 V for (b–d) vs RHE, respectively. Corresponding CV profiles of O_2 reduction are shown in (e–h). Reprinted with permission from Refs. 111, Copyright American Chemical Society (2003) and (2004).

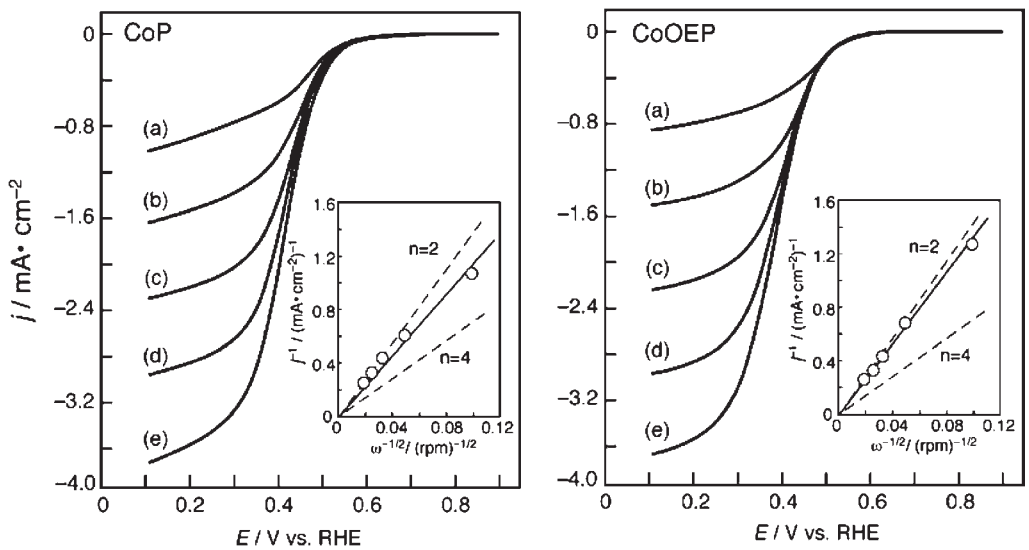

Fig. 7. Current–potential curves for the O_2 reduction at rotating CoP- (left) and CoOEP- (right) modified Au(111) disk electrodes in 0.1 M $HClO_4$ saturated with O_2. Insets show Koutecky–Levich plots. The potential scan rate was 10 $mV\,s^{-1}$. Reprinted with permission from Ref. 111a, Copyright American Chemical Society (2004).

cules formed three packing arrangements on Au(111) surface, i.e., one rectangular arrangement on reconstructed Au(111) and two hexagonal arrangements on Au(111)–(1 × 1), depending on the surface coverage.[111c] The packing arrangement of CoPc on the reconstructed Au(111) surface was also consistent with that obtained in UHV by Lu and co-workers.[101] On the other hand, when the CoPc adlayer was prepared by immersing Au(111) in the benzene solution for 20 min, reconstructed rows of Au(111) under highly ordered arrays of CoPc were no longer seen. The terrace was completely covered with highly ordered domains with two different hexagonal packing arrangements of CoPc, i.e., the adlayer structures of CoPc on Au(111)–(1 × 1) were composed of $c(5 \times 6\sqrt{3})rect$ and $(3\sqrt{3} \times 3\sqrt{3})R30^\circ$ structures.[111c] Figure 6d shows a typical STM image of a CoPc adlayer with $(3\sqrt{3} \times 3\sqrt{3})R30^\circ$ symmetry on Au(111)–(1 × 1) surface.

The enhancement of reductive current for O_2 reduction at CoPor- or CoPc-modified Au(111) electrode compared to that at the bare Au(111) electrode clearly shows that the CoPor and CoPc adlayers catalyze the reduction of O_2 (see Figs. 6e–6h). Use of rotating CoPor-modified Au(111) disk electrodes indicated that the two-electron reduction process of O_2 to H_2O_2 proceeded on the CoP-, CoOEP-, CoTPP-, and CoPc-modified Au(111) surfaces, as shown in Fig. 7.[111] Peak potentials of O_2

Table 2. Potential of O_2 Reduction and Surface Concentration of Each Adlayer in 0.1 M $HClO_4$

Por (Pc)	E/V (vs RHE)	Γ/mol cm^{-2}
CoP	0.32	1.44×10^{-10}
CoOEP	0.31	8.7×10^{-11}
CoTPP	0.32	8.4×10^{-11}
CoPc	0.21	8.5×10^{-11}

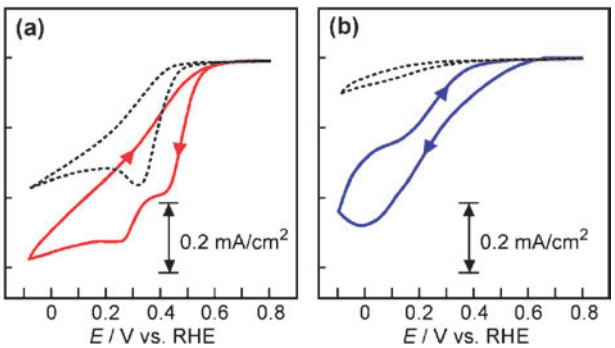

Fig. 8. Cyclic voltammograms of CoOEP- (dotted line) and FeClOEP- (solid line) modified Au(111) electrodes in 0.1 M $HClO_4$ in O_2 atmosphere (a) and in the presence of 10 mM H_2O_2 (b), respectively. The potential scan rate was 50 mV s^{-1}. Reprinted with permission from Ref. 112, Copyright American Chemical Society (2004).

reduction and surface concentration for each adlayer are summarized in Table 2.

Although those adlayers were stable even at potentials near the H_2 evolution potential, the electrochemical reduction of O_2 revealed not four-electron reduction but two-electron reduction of O_2 proceeded only to H_2O_2 with the transfer of two electrons, not to H_2O with the transfer of four electrons. On the FeClOEP adlayer on Au(111) surface, the O_2 reduction was examined in 0.1 M $HClO_4$ saturated with O_2.[112] As can be seen in Fig. 8a, a clear difference in electrocatalytic activity exists between the CoOEP- and the FeClOEP-modified Au(111) electrodes. On the CoOEP-adsorbed Au(111) electrode (dotted line), the catalytic current of O_2 commenced at ca. 0.5 V during the cathodic scan, and a clear reduction peak was observed at 0.32 V, as shown in Fig. 6f. At potentials more negative than 0.3 V, the reductive current remained almost constant because of the process being limited by the diffusion of O_2. It was estimated from the current density (ca. 0.4 mA cm^{-2}) that the two-electron reduction of O_2 to H_2O_2 occurred on the CoOEP-modified Au(111) electrode. On the other hand, the CV profile of FeClOEP-modified Au(111) electrode (solid line, Fig. 8a) was quite different from that of CoOEP (dotted line). On the FeClOEP-adsorbed Au(111) electrode, the catalytic current of O_2 commenced at ca. 0.6 V during the cathodic scan, and two electrocatalytic reduction peaks were observed clearly at 0.45 and 0.25 V. From the current density, it can be roughly estimated that the two-step four-electron reduction of O_2 to H_2O occurred at the FeClOEP-modified Au(111) electrode. We next examined the electrochemical reduction of H_2O_2 at both the CoOEP-modified and the FeClOEP-modified Au(111) electrodes. In this case, the difference in electrochemical activity between CoOEP-modified and FeClOEP-modified

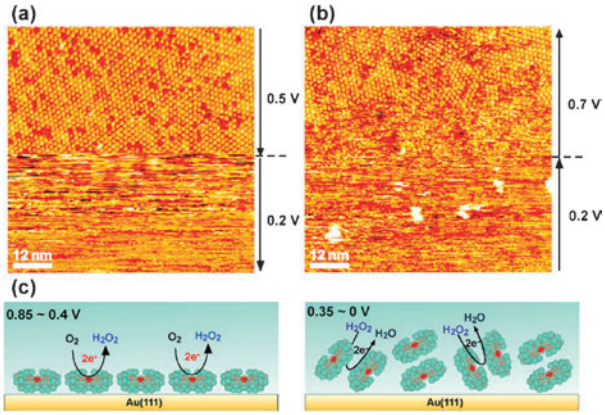

Fig. 9. Composite STM images of the FeClOEP adlayer on Au(111) surface in 0.1 M $HClO_4$ acquired at 0.2 V, after stepping the potential from (a) 0.5 V and returning to (b) 0.7 V, respectively. Potential of the tip and tunneling current were 0.45 V and 1.5 nA, respectively. (c) Proposed models for the FeClOEP adlayer on Au(111) surface in 0.1 M $HClO_4$. Reprinted with permission from Ref. 112, Copyright American Chemical Society (2004).

Au(111) electrodes was very clearly observed, as shown in Fig. 8b. While no peak was seen at the CoOEP-modified Au(111) electrode, a reductive peak appeared at 0 V at the FeClOEP-modified Au(111) electrode. The observed current density shows that two electrons passed at 0 V, i.e., the electrochemical reduction of H_2O_2 to H_2O took place on the FeClOEP-modified Au(111) electrode.

To investigate the stability of FeClOEP adlayer on Au(111) surface in 0.1 M $HClO_4$, we examined the dependency of the adlayer structure on potential. Highly ordered adlayers of FeClOEP which are identical to those of CoOEP were consistently observed in the potential region between 0.9 and 0.4 V. Composite STM images were recorded by stepping the electrode potential, as shown in Fig. 9a. When the electrode potential was stepped from 0.4 to 0.2 V in the middle of scanning, the STM image became unclear. The adlayer of FeClOEP immediately disappeared, as shown in the lower part of Fig. 9a. No electrochemically induced reconstruction of Au(111) was observed at this potential, suggesting that FeClOEP molecules did not desorb from the Au surface but became highly mobile on the surface. Two min later, the electrode potential was returned to 0.7 from 0.2 V. An identical structure was again formed on the terrace, as shown in the upper portion of Fig. 9b. In the potential region between 0.4 and 0 V, a face-to-face dimer of FeClOEP molecule might have formed near the Au surface because of the high mobility of the adsorbed FeClOEP molecules, as illustrated in the proposed model in Fig. 9c. As described above, a highly ordered adlayer of CoOEP was consistently observed in the potential region between 0 and 0.95 V. Although further investigation is needed, the observed effect of potential switching clearly demonstrates that the stability of the MOEP adlayer on Au(111) depends upon the central metal ion. The stability of adlayers on the electrode surface might be one of important factors controlling the electrochemical activity for the reduction of O_2.[112]

3.2 Crown Ether-Substituted Pc Array. The method of

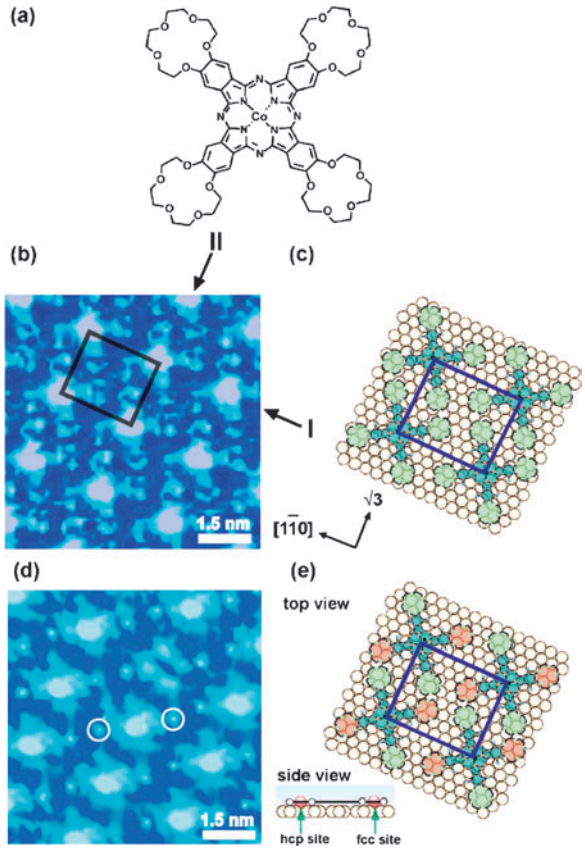

Fig. 10. (a) Molecular structure of CoCRPc. (b–e) High-resolution STM images and models of CoCRPc arrays on Au(111) surface in 0.05 M $HClO_4$: (b) and (c) in the absence and (d) and (e) in the presence of 1 mM Ca^{2+}, respectively, acquired at (b) 0.85 and (d) 0.8 V vs RHE. Potential of the tip and tunneling current were (b) 0.45 V and 1.0 nA and (d) 0.35 V and 5.0 nA, respectively. Model (c) is for the CoCRPc adlayer on Au(111) surface with a superimposed $p(8 \times 4\sqrt{3}R - 30^\circ)$ unit cell, and model (e) is for the CoCRPc array complexed with Ca^{2+} on Au(111) surface with a superimposed $p(8 \times 4\sqrt{3}R - 30^\circ)$ unit cell. Note that the STM image for panel (d) was shown by rotating original STM image in order to fit the direction of molecular row with that in panel (b). Reprinted with permission from Ref. 113b, Copyright American Chemical Society (2004).

immersion into benzene solution was further extended to a larger molecule such as 15-crown-5-ether-substituted phthalocyaninatocobalt(II) (CoCRPc) (see Fig. 10a).[113] It is important to understand host–guest recognition at the electrochemical interface for designing functional electrode with high selectivity. To our knowledge, the inclusion of alkali metal ions in crown ethers on electrodes in solution had not been directly observed by in situ STM. Adlayers of CoCRPc were prepared by immersion of either Au(111) or Au(100) substrate into benzene-ethanol (9:1 v/v) mixed solutions containing CoCRPc. In situ STM imaging was carried out after transferring the CoCRPc-modified Au crystals into aqueous $HClO_4$ solution. Figure 10b shows a typical high-resolution STM image. It is clear that the CoCRPc molecules formed a well-ordered adlayer on Au(111). In addition to the information concerning the symmetry and the structure of CoCRPc arrays, this STM image reveals a great deal of information concerning the internal molecular structure. The shape of the observed features in the image is reminiscent of the molecular structure of CoCRPc. Each molecule can be seen as propeller-shaped with the brightest spot at the center, with four additional bright rings at the corners of each CoCRPc molecule. All molecules are oriented in the same direction on Au(111). The corners of each CoCRPc molecule are seen to be arranged in side-by-side configuration, i.e., crown rings of nearest neighbor molecules are closely positioned with respect to each other. The packing arrangement of the CoCRPc array on Au(111) was determined to be $p(8 \times 4\sqrt{3}R - 30^\circ)$, as illustrated in Fig. 10c. CoCRPc is known to form dimers in solution phase in the presence of alkali metal ions such as Na^+, K^+, and Ca^{2+}.[114] To investigate host–guest complexation with those ions on the CoCRPc-modified Au(111) surface, a 0.05 M $HClO_4$ solution containing 10 mM Ca^{2+} was added dropwise into the electrochemical STM cell after the formation of a well-defined adlayer of CoCRPc was confirmed in pure 0.05 M $HClO_4$ by STM. The concentration of Ca^{2+} in the STM cell was ca. 1 mM. Figure 10d shows STM images of a CoCRPc adlayer formed on the Au(111) surface after adding Ca^{2+} ions. Each CoCRPc molecule exhibits a characteristic shape with the brightest spot at the center, except for the molecule located on the left of the center of the image, in which the central metal appears to be missing. In the absence of Ca^{2+}, four additional spots were observed at the corners, whereas in the presence of Ca^{2+}, only two additional bright spots were observed at diagonal positions with respect to the Pc ligand, as marked by two circles in Fig. 10d, as a result of encapsulation of two Ca^{2+} ions by crown ether rings. A schematic model is presented in Fig. 10e. In this model, central Co^{2+} ions are located at 2-fold bridge sites, but the diagonal axes of CoCRPc are rotated by ca. 10° with respect to the direction of Au atomic row (Fig. 10d). With this rotational angle, the centers of the two crown ether moieties, which are shown in red, are situated at hcp and fcc 3-fold hollow sites, whereas the other two unoccupied moieties, colored green, are at near bridge sites. The rotation of molecules upon complexation with Ca^{2+} might have been caused by a change in interaction between the crown ether moieties in neighboring molecules. It might also be possible that crown ethers with Ca^{2+} ions favor three-fold sites, as depicted in the side view in Fig. 10e. The distance between the Au lattice and crown moieties probably plays a significant role in the host–guest recognition. On the other hand, two adlayer structures of CoCRPc, (8×9) and $(4\sqrt{5} \times 4\sqrt{5})R26.7^\circ$, were found on Au(100)–$(1 \times 1)$ terrace. In the presence of 1 mM Ca^{2+}, two Ca^{2+} ions were trapped in two diagonally located 15-crown-5-ether moieties of each CoCRPc molecule on Au(111), whereas encapsulation of Ca^{2+} ions was not seen in the CoCRPc arrays on Au(100)–(1×1) surface. The result demonstrates that the relationship between crown moieties of CRPc and the underlying Au lattice is important in the trapping of Ca^{2+} ions in crown rings.[113b]

3.3 Controlled Binary Arrays. Self-assembly of complementary subunits via non-covalent interactions such as hydrogen bonds is an attractive approach to the controlled oligomerization of monomers to form large supramolecular architec-

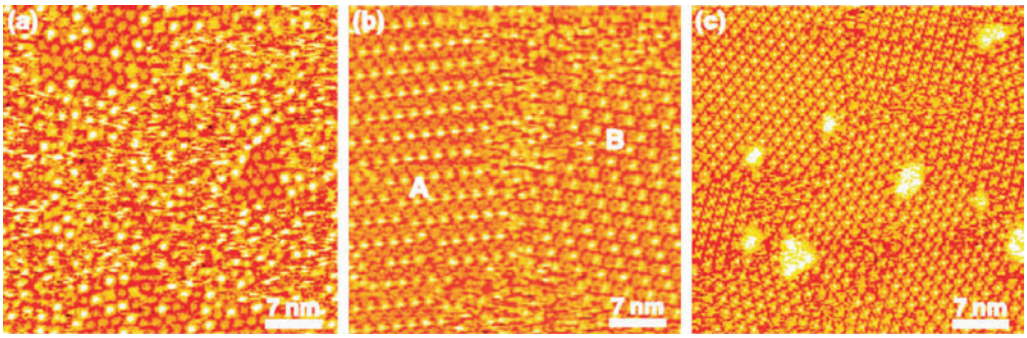

Fig. 11. Typical large-scale ($40 \times 40\,nm^2$) STM images, acquired at 0.85 V vs RHE in 0.1 M $HClO_4$, of CuOEP and CoPc binary arrays on Au(111) prepared by immersion in ca. 3 μM CuOEP benzene solution saturated with CoPc. The immersion times were (a) 4, (b) 6, and (c) 20 min, respectively. The tip potential was (a) 0.45, (b) 0.47, and (c) 0.35 V vs RHE. Tunneling currents were (a) 0.8, (b) 2.0, and (c) 10 nA, respectively. Reprinted with permission from Ref. 116a, Copyright American Chemical Society (2004).

tures. For example, the supramolecular nanostructures composed of carboxyphenyl-substituted porphyrin on Au(111) can be precisely controlled by the conformation selective assembly.[31b] We recently investigated the organization and hydrogen-bonding network formation of carboxyphenyl porphyrin derivatives at electrochemical interfaces. Our results demonstrated that the ordered arrays of monocarboxy- or tetracarboxy-substituted porphyrin derivatives formed on a Au(111) surface in acidic solution depend to a remarkable extent both on the number of peripheral substituents and on the modulation of the applied potential, and that electrochemical control of the self-assembly of porphyrin complexes is an effective method for constructing novel surface architectures.[104] The binary system consisting of porphyrin and phthalocyanine will help for the understanding supramolecular design of nanoarchitectures. As mentioned above, porphyrins are also well-known as suitable building components to construct two- or three-dimensional self-organizations of multiarrays. Hipps et al. found the formation of well-ordered regions with an entirely new structure with 1:1 composition of hexadecafluorophthalocyaninatocobalt(II) (F_{16}CoPc) and NiTPP on Au(111) by vapor-phase deposition in UHV.[104a] F_{16}CoPc and NiTPP molecules were distinguished from each other by the difference in brightness of central metal ions between F_{16}CoPc and NiTPP molecules. The remarkable contrast in tunneling current afforded by the difference in electronic configuration of transition-metal ions allows one to clearly discriminate between species for chemical identification at the molecular level. When CoPc and NiTPP molecules were deposited on Au(111), a densely packed and well-ordered structure was also found on the terrace. However, the binary adlayer consisting of CoPc and NiTPP prepared in UHV revealed a densely packed, apparently well-defined structure, which is compositionally disordered.[104b] Hipps et al. concluded that the formation of 1:1 composition of F_{16}CoPc and NiTPP is explained by the ability of the two types of molecules to interlace, the up-to-4 kJ mol^{-1} attractive energy for each close-approach fluorine–hydrogen intermolecular interaction and by the reduced repulsive interaction between F_{16}CoPc molecules because of the increase of spacing forced by NiTPP units.

A bimolecular system consisting of CuOEP and CoPc on Au(111) was examined by our group.[116a] The CuOEP and CoPc binary adlayers were prepared on Au(111) surface with varying immersion times in the benzene solution. Figures 11a–11c show typical STM images of the binary adlayers formed on Au(111) at immersion times of 4, 6, and 20 min, respectively. As can be seen in Fig. 11a, the adlayer at the immersion time of 4 min was composed of well-ordered and disordered segments over the entire surface of the terrace. The well-ordered portion was composed of hexagonally packed CuOEP molecules. The adlayer structure prepared with a short immersion time (less than 2 min) revealed that a CuOEP adlayer was formed predominantly on Au(111), suggesting that CoPc molecules displace the CuOEP molecules during the modification process with increasing immersion times. It is demonstrated that the molecular assembly of CuOEP on Au surface forms more quickly than that of CoPc. When the modification with CuOEP and CoPc was allowed to continue for 6 min, a completely different, new domain appeared on the terrace, as shown in Fig. 11b. The terrace was now covered with two different domains. Highly ordered molecular rows were clearly recognized as stripes consisting of bright and dark lines. Each molecular row consisting of stripes runs parallel to the so-called $\sqrt{7}$ direction of Au(111) lattice. Molecular rows between two domains A and B crossed each other at an angle of ca. 108°. Molecular rows in both domains are aligned along the $\sqrt{7}$ direction of the Au(111) lattice, but the relationship between the two domains is such that they constitute a set of rotational mirror images. When the immersion time was longer than 20 min, the terrace was completely covered with CoPc molecules only. Careful inspection of the highly ordered arrays of CoPc molecule formed on the Au(111)–(1×1) reveals that islands are often observed at domain boundaries, as shown in Fig. 11c.

Figure 12 shows the high-resolution STM images of alternate molecular rows consisting of CuOEP and CoPc molecules. A high-resolution STM image obtained in domain A in Fig. 11b is displayed in Fig. 12a. Individual CoPc molecules in the row marked by arrow I are propeller-shaped with the brightest spot at the center and four additional spots at the corners. It is clear that all CoPc molecules are oriented in the same direction on Au(111). On the contrary, each molecule in the dark row marked by arrow II is in the shape of a ring with a central dark spot, indicating that it is a CuOEP. The difference

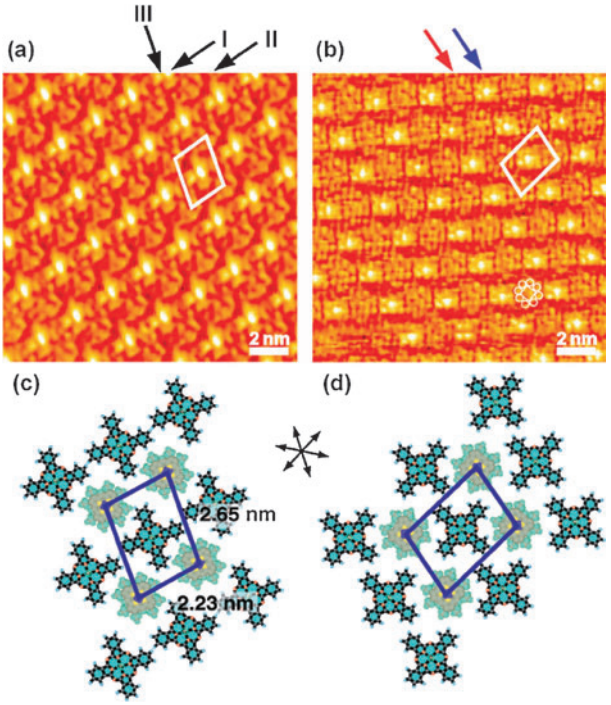

Fig. 12. (a and b) High-resolution ($15 \times 15\,nm^2$) STM images of alternate binary CuOEP and CoPc array on Au(111) surface in 0.1 M $HClO_4$ acquired at 0.85 V vs RHE and (c and d) corresponding proposed models. Tip potentials and tunneling currents were 0.35 V and 5.5 nA for (a) and 0.45 V and 0.85 nA for (b), respectively. Structural models are for the CuOEP and CoPc binary adlayers on Au(111) surface with superimposed (c) $p(9 \times 3\sqrt{7}R - 40.9°)$ and (d) $p(9 \times 3\sqrt{7}R - 19.1°)$ unit cells. The set of three arrows indicate lattice directions of Au(111) substrate. Reprinted with permission from Ref. 116a, Copyright American Chemical Society (2004).

in brightness at the centers of CoPc and CuOEP molecules is clearly explained by the difference in the mode of occupation of d orbitals.[101,103] From the cross-sectional profile, the intermolecular distance between CoPc molecules aligned in the direction of arrow I (Fig. 12a) and that between CuOEP molecules aligned in the direction of arrow II were both measured to be 2.23 ± 0.06 nm, whereas the distance between CoPc molecules aligned in the direction of arrow III was found to be 2.63 ± 0.08 nm. These values correspond to $3\sqrt{7}$ and 9 times the Au lattice constant, respectively. An adlattice is superimposed with solid lines in Fig. 12a. When the usual tunneling current lower than 1 nA was used, the molecular row of CuOEP indicated by the red arrow in Fig. 12b was clearly resolved as a well-defined chemical structure. On the contrary, the shape of each CoPc molecule in the rows indicated by the blue arrow was variant under these conditions. The adlattice of the two-component adlayer consisting of CuOEP and CoPc shown in Fig. 12b was identical to that shown in Fig. 12a, however. It has a $p(9 \times 3\sqrt{7}R - 19.1°)$ structure, which is a mirror image of $p(9 \times 3\sqrt{7}R - 40.9°)$. Structural models of $p(9 \times 3\sqrt{7}R - 40.9°)$ and its mirror image structure, $p(9 \times 3\sqrt{7}R - 19.1°)$, are proposed in Figs. 12c and 12d, respectively.

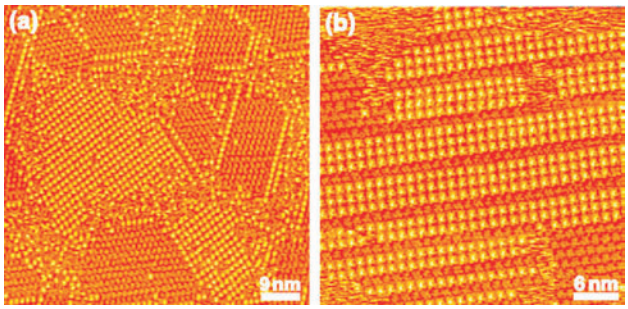

Fig. 13. Typical STM images of binary CuOEP and CoPc arrays on Au(111) surface in 0.1 M $HClO_4$ acquired at (a) 0.45 and (b) 0.65 V after stepping the potential from 0.85 V. Potential of the tip and tunneling current were 0.35 V and 4.5 nA, respectively. Reprinted with permission from Ref. 116a, Copyright American Chemical Society (2004).

We attempted to control the domain size and composition by the potential scan at a slow rate to a slightly anodic potential. Figure 13a shows a typical STM image of a CuOEP and CoPc adlayer formed on the Au(111) surface after the potential was held constant at 0.45 V following the scan from 0.8 V at a scan rate of $10\,mV\,s^{-1}$. This STM image shows that the structure changed drastically upon this potential manipulation, i.e., the alternate packing structure of binary CuOEP and CoPc disappeared, and a new structure was formed on the terrace, in which arrays of bright domains with square lattice and dark domains with quasi-hexagonal lattice were arranged alternately. In the bright domain composed of CoPc molecules, a highly ordered array with square packing arrangement was found. Also, bright CoPc molecular rows ran parallel to the CuOEP domain. Figure 13b shows a typical STM image of a mixed CuOEP and CoPc adlayer formed on the Au(111) surface after the potential was held at 0.65 V for 30 min. In this case, one-dimensional (1D) molecular chains of CuOEP were clearly observed as dark gaps between bright rows consisting of two or three CoPc molecular rows. These results show that the adlayer structure depends strongly upon electrochemical potential, suggesting that potential modulation is a key factor controlling alternate CuOEP and CoPc molecular chains. The similar ordering of porphyrins at negative potentials was reported by Borguet et al. to result from a change in surface interactions.[109] The reason why the phase separation takes place is not clear. One possible reason is the difference in charge distribution resulting from either central metal ion (Cu ion and Co ion) or chemical framework (OEP and Pc). In this system, the surface mobility and the molecular re-organization of CuOEP and CoPc were accelerated by modulation of electrode potential. The surface charge density at electrochemical interface would contribute not only to the interaction between molecule and substrate but also to the interaction between molecules.

Another system, a bimolecular array consisting of CoPc and CuTPP, was examined both on Au(111) and Au(100) in the same manner. We found that an alternate mixed layer consisting of CoPc and CuTPP was formed on reconstructed Au(100)–(hex) but not on reconstructed Au(111), suggesting that the supramolecular assembly consisting of two chemical components also depends upon the crystallographic orientation

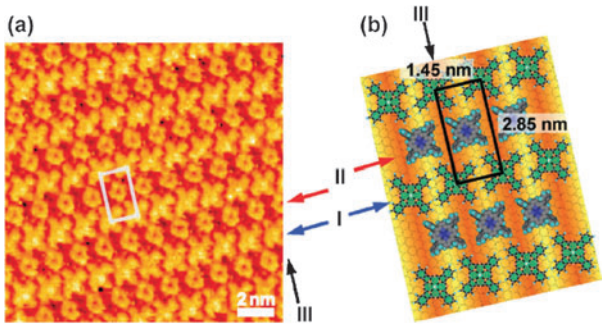

Fig. 14. (a) High-resolution STM image ($15 \times 15\,nm^2$) and (b) structural model of CoPc and CuTPP mixed adlayer formed on Au(100)–(hex) surface in 0.1 M $HClO_4$ acquired at 0.75 V versus RHE. Potential of the tip and tunneling current were 0.45 V and 1.2 nA, respectively. Reprinted with permission from Ref. 116b, Copyright American Chemical Society (2003).

of Au.[116b] In this case, the terrace of Au(111) was completely covered with two different phases: disordered region and highly ordered region consisting of CuTPP, whereas the stripes composed of alternate bright and dark lines were observed on Au(100)–(hex). Details of the internal structure, orientation and packing arrangement of the binary CoPc and CuTPP adlayer on Au(100)–(hex) are seen in the high-resolution STM image shown in Fig. 14a. It can be seen that alternate molecular rows are uniformly formed on Au(100)–(hex). An individual CoPc molecule marked by arrow I can be recognized as a propeller-shaped image with a central brightest spot and four additional spots at the corners. These bright spots can be attributed to the benzene moieties in the CoPc molecule as reported in our previous paper.[111c] On the basis of the cross-sectional profile, the intermolecular spacing between CoPc molecules and between CuTPP molecules aligned in the directions of arrow I and II were both measured to be 1.44 ± 0.05 nm, whereas the distance between CoPc molecules indicated by arrow III was found to be 2.85 ± 0.07 nm. These two values correspond to almost 5 and 10 times the Au lattice constant, respectively. A structural model of CoPc and CuTPP mixed adlayer formed on the Au(100)–(hex) surface is presented in Fig. 14b. We subsequently found that each CuTPP molecule is likely to be in the higher part in reconstructed rows, whereas each CoPc molecule is likely to be located in the lower part of reconstructed rows at lower coverage of those molecules. Therefore, each molecule can alternately locate on bright and dark parts of reconstructed rows of Au(100)–(hex).[117] This excellent finding might be tentatively explained by fitting between adlattices consisting of two component molecules (molecular packing arrangement) and periodicity of reconstructed row of Au(100)–(hex).

As mentioned above, the adlayer structure depends strongly upon the underlying Au lattice, suggesting that the reconstructed Au(100)–(hex) surface is a key factor in controlling alternate CoPc and CuTPP molecular chains. The binary adlayers of CoPc and CuTPP might be controllable either by the difference in potential of zero charge between Au(111)–$(\sqrt{3} \times 22)$ and Au(100)–(hex) or by the underlying reconstructed structure of Au. Although further investigations of the dependence on the crystallographic orientation are needed, a clear difference between bimolecular adlayers on Au(111) and those on Au(100) surfaces was found by using the wet deposition method. Such a precise and unique control on metal substrate is of great interest for further applications of porphyrin and phthalocyanine molecular assemblies.

4. Supramolcular Assembly Consisting of Fullerene and Porphyrin

It is known that porphyrins and fullerenes are spontaneously attached to each other.[118] For example, MOEP and C_{60} form a supramolecular assembly through the π–π interaction in cocrystallites with a ratio of 2:1.[118b] To control supramolecular assemblies between porphyrins and fullerenes is important for three-dimensional construction by layer-by-layer growth on metal surfaces as a first step. Such a supramolecular assembly produced through π–π or donor–accepter interaction would be useful for the design and organization of functional organic molecules on electrode surfaces. From the viewpoint of photo electron-transfer reaction, zinc-coordinated porphyrins are often used in the related research fields.[28] We also found that highly ordered adlayers of octaethylporphyrinatozinc(II) (ZnOEP), tetraphenylporphyrinatozinc(II) (ZnTPP), and phthalocyaninatozinc(II) (ZnPc) can be formed on Au(111) by benzene immersion method.[119]

Here, we describe the formation of 1:1 fullerene–porphyrin supramolecular assemblies of not only C_{60}[120] but also its functional derivatives such as open-cage C_{60} (opened C_{60})[121] and ferrocene-linked C_{60} (C_{60}Fc)[122] on a highly ordered ZnOEP array formed on Au(111) and reconstructed Au(100)–(hex) surfaces; these exhibit a well-defined electrochemical response.

4.1 Control of Molecular Orientation of Fullerenes on ZnOEP Array. Figure 15a shows typical CVs of a ZnOEP-modified Au(111) (dotted line) and C_{60} on the ZnOEP-modified Au(111) electrode (red solid line) in 0.1 M $HClO_4$ recorded at a scan rate of 50 mV s^{-1}. For ZnOEP-modified Au(111)

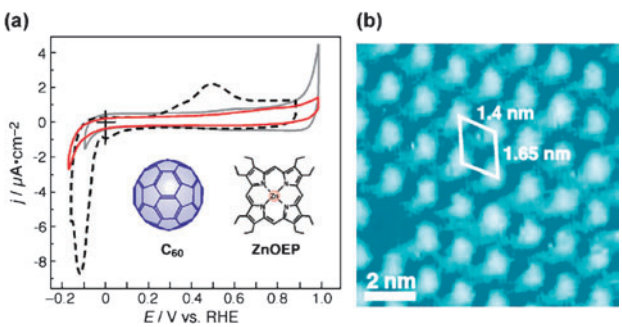

Fig. 15. (a) Cyclic voltammograms of C_{60} directly attached Au(111) (gray line) and ZnOEP-modified on Au(111) electrode in 0.1 M $HClO_4$ before (dotted line) and after (red solid line) immersion into a C_{60} benzene solution. The scan rate was 50 mV s^{-1}. (b) Typical STM image of C_{60} on the ZnOEP-modified on Au(111) electrode acquired at 0.8 V vs RHE in 0.1 M $HClO_4$. Tip potential and tunneling current were 0.46 V and 0.55 nA. Reprinted with permission from Ref. 120, Copyright The Chemical Society of Japan (2004).

electrode, potential scan was started to the negative direction from open circuit potential (around 0.75 V). During the scan to more negative direction, a reductive peak was seen around −0.1 V, whereas a reoxidative peak was observed around 0.5 V, suggesting that reductive desorption and re-adsorption of ZnOEP molecule took place on the Au(111) surface. Immersion into ca. 10 μM C_{60} benzene solution was further carried out for some time after the ZnOEP modification onto the Au(111) surface. The decrease in double-layer charging current was observed, and the peaks observed around −0.1 and 0.5 V were suppressed as indicated by the red solid line, whereas the increase of anodic current can be seen at 0.9 V on C_{60}-modified Au(111) electrodes because of the oxidative desorption of C_{60} molecules, as indicated by the gray line.[51a] This result suggests that the ZnOEP adlayer on Au(111) surface prevents the oxidative desorption of C_{60} molecules.

Highly ordered C_{60} arrays consisting of bright round spots were found on the ZnOEP-modified Au(111) in the high-resolution STM image of an area of $10 \times 10\,nm^2$ as shown in Fig. 15b. As reported in several papers, the epitaxial thin film of C_{60} on Au(111) was found to take two different close-packed structures, $(2\sqrt{3} \times 2\sqrt{3})R30^\circ$ and the so-called "in-phase" (38×38), not only in UHV[123] but also in solution.[51a,124] The intermolecular distance between C_{60} molecules was 1.0 nm. The size of each spot on the ZnOEP-modified Au(111) was larger than that directly attached on Au(111), suggesting that the underlying ZnOEP layer affects the electronic structure of C_{60} molecules. On the basis of cross-sectional profiles, intermolecular distances between the nearest neighbor C_{60} molecules were found to be either 1.65 ± 0.07 or 1.40 ± 0.05 nm for directions along each molecular row. The corrugation height of C_{60} was clearly greater than that of the ZnOEP layer on Au(111). The underlying ZnOEP layer on Au(111) was clearly visible at an increased tunneling current and/or when the bias potential was changed. Actually, the top layer of C_{60} was easily removed with the operation of scanning at tunneling currents higher than 0.5 nA. Figure 16a shows a typical STM image obtained after scanning with tunneling current of 1 nA. Highly ordered C_{60} molecules of the top layer disappeared. Clusters of C_{60} were formed by such a higher tunneling current during the scan of tip, whereas the underlying ZnOEP first layer was clearly observed under this experimental condition. The result indicates that the interaction between C_{60} and ZnOEP adlayer is quite weak. A close-up view of underlying ZnOEP layer is shown in Fig. 16b. Careful inspection of Fig. 16b allows one to distinguish between two different orientations of ZnOEP molecules in the molecular rows. Each ZnOEP molecule can be recognized as a square with eight additional spots at the corners corresponding to eight ethyl groups. The adlayer structure of ZnOEP on Au(111) was identical to that of CoOEP on Au(111) as described in previous section. Note that the ZnOEP adlayer was the same as that before C_{60} adsorption. Although the unit cell is superimposed in Fig. 16b as the parallelogram with the length of 1.62 and 2.81 nm because of two different orientations of ZnOEP molecules, intermolecular spacings between the molecules in the rows in Fig. 16b were measured to be 1.65 ± 0.07 and 1.40 ± 0.05 nm. In the case of C_{60}, 1:1 supramolecular assembled layer of C_{60} and ZnOEP could be also formed on Au(111) surface. The fact that the intermolecular distances between C_{60} molecules are nearly equal to the distance between ZnOEP molecules indicates that each C_{60} is located on the center above each ZnOEP molecule. The identical structures of C_{60} and C_{70} were also observed on NiOEP array formed on Au(111).[125] However, the replacement reaction of the first adlayer of tetraphenylporphyrinatonickel(II) (NiTPP) occurred upon adsorption of fullerene molecules as the second layer, suggesting that supramolecular assemblies of C_{60} and C_{70} are strongly influenced by the underlying layer of porphyrin. The dependency on the underlying porphyrin layer for supramolecular assembly of fullerenes might be tentatively explained by the difference in interaction between porphyrin and fullerene. According to the density functional theoretical (DFT) calculation, the interaction energy between ZnTPP and C_{60} was estimated to be −16 to −18 kcal mol^{-1},[126] whereas that between ZnP (not ZnOEP) and C_{60} was −33.9 kcal mol^{-1}.[127] It was demonstrated that the stability of the first adlayer is an important factor in the surface design of host–guest selectivity of fullerenes on electrode surfaces. Bonifazi et al. synthesized porphyrinatozinc dimer and investigated supramolecular assembly of C_{60} on the porphyrinatozinc dimer array formed on Ag(100) in UHV environment.[128] Such π-conjugated molecules with tunable electronic properties are building blocks for the construction of functional materials with exceptional electrochemical and photophysical properties. C_{60} molecules located precisely on top of the 3-cyanophenyl substituents in porphyrinatozinc dimer array. Supramolecular assembly of C_{60} also depended upon chemical structures in the underlying porphyrin layer or the metal substrates. It is noteworthy that the control of supramolecular assembly of fullerenes has been extended to another system. Supramolecularly assembled layers of C_{60} and its dimer derivatives were examined on both coronene- and perylene-modified Au(111) surfaces.[129] As reported in our previous papers, coronene formed a highly ordered array having a (4×4) symmetry on Au(111).[50] The adlayer structure of the C_{60} was found to be strongly influenced by the underlying organic layers, suggesting that the latter underlying organic adlayers play an impor-

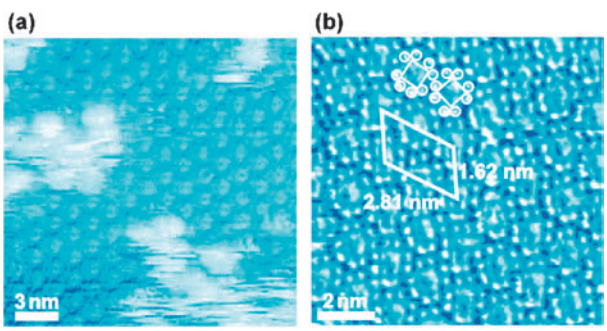

Fig. 16. Typical high-resolution STM images ($10 \times 10\,nm^2$) of C_{60} array on (a) clean Au(111) and (b) the ZnOEP-modified on Au(111) surface acquired at 0.85 V vs RHE in 0.1 M $HClO_4$. Tip potential and tunneling current were 0.46 V and 1.0 nA for (a) and 1.5 nA for (b), respectively. Reprinted with permission from Ref. 120, Copyright The Chemical Society of Japan (2004).

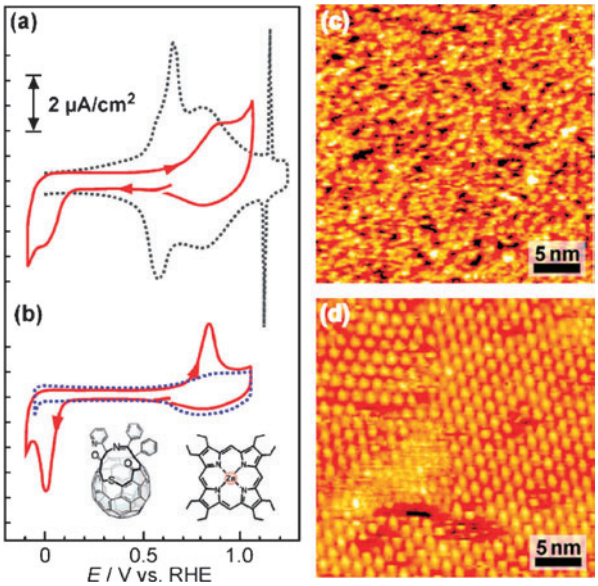

Fig. 17. Typical cyclic voltammograms of (a) bare Au(111) (dotted line) and opened C_{60}-adsorbed Au(111) (solid line), and (b) ZnOEP-adsorbed (dotted line) and opened C_{60}/ZnOEP-adsorbed (red solid line) Au(111) electrodes in pure 0.05 M H_2SO_4. The scan rate was 20 mV s^{-1}. Typical large-scale STM images ($30 \times 30\,nm^2$), acquired at 0.85 V vs RHE, of opened C_{60} adlayer directly formed on Au(111) and on ZnOEP-modified Au(111) in 0.05 M H_2SO_4 are shown in (c) and (d), respectively. The tip potentials and tunneling currents were 0.44 V and 0.5 nA for (c), and 0.31 V and 0.3 nA for (d), respectively. Reprinted with permission from Ref. 121a, Copyright Wiley-VCH (2004).

tant role in the process of formation of the C_{60} molecular adlayer.

This approach is more effective for control of molecular orientation of unsymmetrical functional fullerenes. For example, open-cage fullerenes are attractive and important molecules for synthesis of a new endohedral fullerene encapsulating molecular hydrogen. Recently, Komatsu's group succeeded in preparing $H_2@C_{60}$ by a strategy of "molecular surgery" in which the fullerene cage is opened and closed after insertion of H_2 gas.[130] Because the opened fullerene has two carbonyl moieties, this electrochemical redox reaction is expected to be useful as a monitor reaction of the modified surface. Figure 17a shows typical cyclic CVs of a well-defined Au(111) (dotted line) and opened C_{60} directly attached on Au(111) electrode (red solid line) in 0.05 M H_2SO_4 recorded at a scan rate of 20 mV s^{-1}. For the Au(111) electrode modified with opened C_{60}, a broad reduction peak was observed in the potential range between 0.1 and −0.1 V, whereas a reoxidation peak appeared at 0.85 V during the anodic scan. The dotted line in Fig. 17b shows CV of a ZnOEP-modified Au(111) electrode in 0.05 M H_2SO_4. No noticeable peak was observed in the potential range between 0 and 0.7 V. After subsequent immersion of the electrode into ca. 50 μM opened C_{60} benzene solution for 1 min, a decrease in double-layer charging current was observed, and a pair of characteristic redox peaks clearly appeared at 0 and 0.85 V during cathodic and anodic scans, respectively. This result suggests that opened C_{60} was attached on the ZnOEP-modified Au(111) surface, and that carbonyl groups of opened C_{60} were oriented toward the solution phase. The CV profile drawn with a solid red line in Fig. 17b is strongly associated with the electrochemical redox reaction of >C=O to >C•–OH (and >C•–OH to >C=O) for two carbonyl groups in each molecule of opened C_{60}. On the basis of the electronic charge calculated from the reductive peak area, the amount of transferred electronic charge is estimated to be ca. 15.8 μC cm^{-2}. If two-electron reduction occurs on the opened C_{60}/ZnOEP-modified Au(111) electrode, the value corresponds to the surface concentration of $(7.9 \pm 0.7) \times 10^{-11}$ mol cm^{-2}. The electron-transfer process is very slow as indicated by the CV profile shown in Fig. 17b. When potential switching was carried out at potentials negative than 0.85 V, no reduction peak at 0 V was observed. Figure 17c shows a typical STM image of an adlayer of opened C_{60} formed on Au(111) in 0.05 M H_2SO_4. This STM image shows a completely disordered structure of opened C_{60} directly attached to the surface of Au(111), while highly ordered arrays consisting of bright round spots were found on the ZnOEP-modified Au(111), as shown in Fig. 17d. Such situation of the modified Au(111) surface was also revealed from CV profile shown in Fig. 17a. This result suggests that a highly ordered adlayer of opened C_{60} was formed not directly on Au(111) but on the ZnOEP-modified Au(111) surface. Further details of the internal structure, orientation and packing arrangement of the supramolecular assembled layers of opened C_{60}/ZnOEP on Au(111) are revealed in the high-resolution STM image. The adlayer structure of opened C_{60} on the ZnOEP-modified Au(111) surface was identical to that of C_{60} on the Au(111) surface covered with highly ordered ZnOEP arrays.

Morphological details of each molecule are clearly displayed in the height-shaded view shown in Fig. 18a. Protrusions were observed in each bright spot, showing the presence of phenyl and pyridyl groups located on the rim of the orifice. When the tunneling current was stepped from 30 pA to 2.0 nA in the middle of scanning, the STM image dramatically changed as shown in Fig. 18b. The adlayer of opened C_{60} immediately disappeared and the underlying ZnOEP layer on Au(111) was visible, indicating that each opened C_{60} molecule was formed on the highly ordered ZnOEP adlayer with 1:1 supramolecular assembly (see Fig. 18c). When a polycrystalline Au electrode such as a disk or a wire was used as a substrate, the redox reaction was not evident even on the opened C_{60}/ZnOEP system. Furthermore, dependency upon the adlayer structures of ZnOEP was found on reconstructed Au(100)–(hex) and unreconstructed Au(100)–(1×1) surfaces.[121b] A hexagonally arranged ZnOEP array was formed on a Au(100)–(hex) surface, whereas rectangularly arranged ZnOEP array was found on a Au(100)–(1×1) surface. The adlayer structure of ZnOEP was depended upon the underlying Au atomic arrangements. Figure 19a shows a typical STM image of an adlayer of opened C_{60} formed on ZnOEP-modified Au(100)–(hex) in 0.05 M H_2SO_4. Highly ordered arrays consisting of bright round spots were observed over the entire surface of Au(100)–(hex). In contrast, a completely disordered structure was observed for the adlayer of opened C_{60} on the ZnOEP-

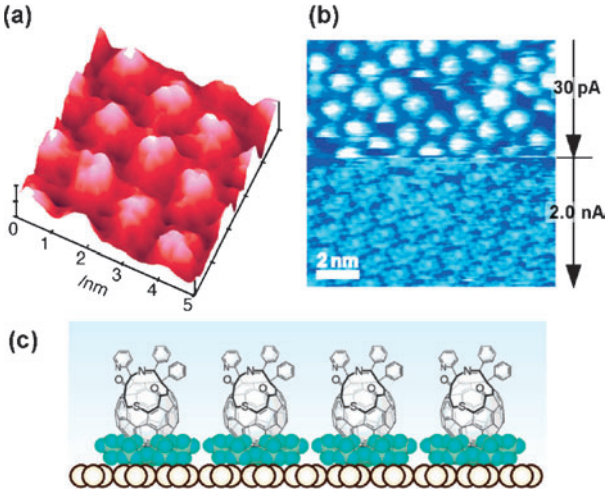

Fig. 18. (a) Height-shaded view of opened C_{60}/ZnOEP supramolecular assembled adlayer on Au(111) in 0.05 M H_2SO_4. The tip potential and the tunneling current were 0.46 V and 0.425 nA, respectively. (b) Composite STM image, acquired at 0.85 V vs RHE, of opened C_{60}/ZnOEP supramolecular assembled layer on Au(111) in 0.05 M H_2SO_4. Potential of the tip was 0.35 V. Tunneling currents were 0.03 nA (upper part) and 2.0 nA (lower part), respectively. (c) Structural model of supramolecular assembled opened C_{60}/ZnOEP adlayer on Au(111). Reprinted with permission from Ref. 121a, Copyright Wiley-VCH (2004).

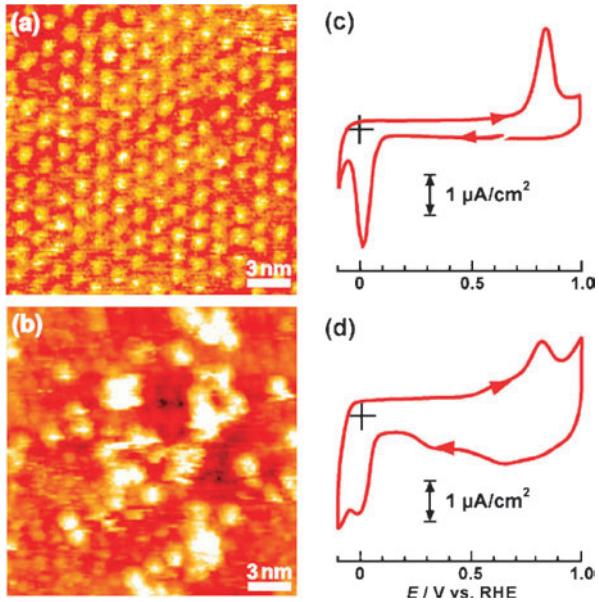

Fig. 19. Typical high-resolution ($20 \times 20\,nm^2$) STM images of the adlayer of opened C_{60} formed on ZnOEP-modified Au(100)–(hex) for (a), and Au(100)–(1 × 1) for (b), all acquired in 0.05 M H_2SO_4. Tip potentials and tunneling currents were 0.46 V and 0.625 nA for (a) and 0.43 V and 0.2 nA for (b), respectively. Corresponding cyclic voltammograms of opened C_{60}/ZnOEP-adsorbed Au(100)–(hex) and Au(100)–(1 × 1) electrodes in 0.05 M H_2SO_4 are shown in (c) and (d), respectively. The scan rate was $20\,mV\,s^{-1}$. Reprinted with permission from Ref. 121b, Copyright American Chemical Society (2005).

modified Au(100)–(1 × 1) surface, as shown in Fig. 19b. Although several individual molecules of opened C_{60} could be distinguished under the present conditions, the ZnOEP-modified Au(100)–(1 × 1) surface was covered largely with aggregates of opened C_{60}, as can be seen. This difference in STM image is clearly reflected in cyclic voltammograms for the modified electrodes. The voltammetric responses for the opened C_{60} on the ZnOEP-modified Au(100)–(hex) surface were similar to that on the ZnOEP-modified Au(111) surface, as shown in Fig. 19c. On the basis of the electronic charge calculated from the reductive peak area, the amount of transferred electronic charge was estimated to be ca. $16.2\,\mu C\,cm^{-2}$, leading to the surface concentration of $(8.4 \pm 0.7) \times 10^{-11}\,mol\,cm^{-2}$. For the opened C_{60} on the ZnOEP-modified Au(100)–(1 × 1) electrode, a pair of broad reduction and re-oxidation peaks was observed during the scan (Fig. 19d). Redox peak currents were smaller than those obtained at Au(100)–(hex) surface, suggesting that the molecular orientation of opened C_{60} was random on the ZnOEP-modified Au(100)–(1 × 1) surface. These results indicate that the carbonyl groups of opened C_{60} were oriented toward the solution phase on the ZnOEP-modified Au(100)–(hex) surface because of the formation of 1:1 supramolecular assembly with highly ordered ZnOEP array. This finding suggests that precise control of underlying ZnOEP adlayers with Au atomic structure is important to recognize the opened C_{60} on them.[121b] The clear enhanced redox peaks in the CV profile at the opened C_{60}/ZnOEP-modified Au(111) and Au(100)–(hex) electrodes strongly support the conclusion that the orientation of opened C_{60} is controlled by the ZnOEP adlayer.

The supramolecular modification is also effective for control of the electron-transfer reaction of ferrocene-linked fullerene (C_{60}Fc).[122] Recently, studies on fullerenes linked to multiple redox and/or photoactive molecular entities have been carried out extensively because they have potentials for constructing supramolecular electronic devices and artificial light energy-generating systems.[9,21,131,132] Especially, because ferrocene is a typical redox species, it is a promising material for an electrochemical switching or sensing device. In the field of electrochemistry, SAM systems using organothiols terminated with an electroactive ferrocene group are most widely employed.[10–12]

Figure 20a shows typical CVs of an Au(111) electrode with directly attached C_{60}Fc in 0.1 M $HClO_4$. They were recorded at a scan rate of $50\,mV\,s^{-1}$. For the Au(111) electrode directly modified with C_{60}Fc, a broad redox peak was observed in the potential range between 0.7 and 1.05 V. The anodic current commencing at 0.95 V is likely to be due to the oxidative desorption of C_{60}Fc molecules from the Au surface, because such an anodic current was also observed at C_{60}- and C_{120}-modified Au(111) electrodes.[51a] The redox current of Fc moiety might be involved in such oxidative current of C_{60} moiety. After subsequent immersion of the ZnOEP-modifed Au(111) electrode into a ca. 50 μM C_{60}Fc benzene solution for 1 min, a decrease in double-layer charging current was observed, and a pair of characteristic redox peaks clearly appeared at 0.78 V during cathodic and anodic scans, respectively (see Fig. 20b). Also, the increase of anodic current commencing at 0.95 V was suppressed by the adsorption of ZnOEP. This result suggests that

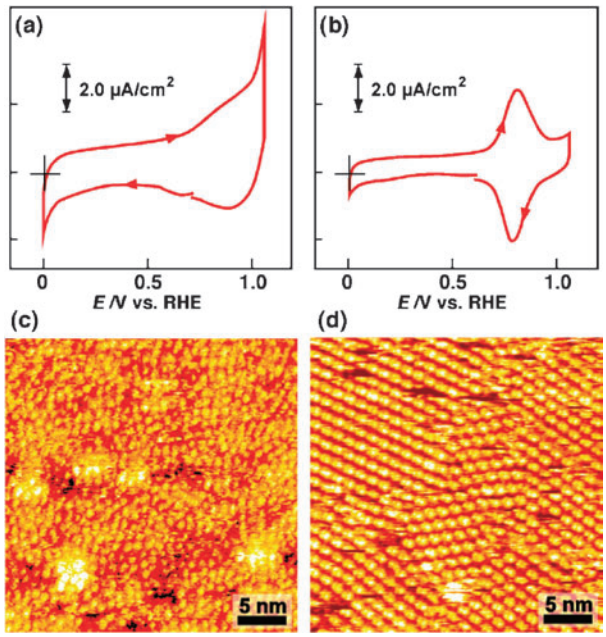

Fig. 20. Cyclic voltammograms of (a) C_{60}Fc-adsorbed Au(111) (red solid line) and (b) C_{60}Fc/ZnOEP-adsorbed (red solid line) Au(111) electrodes in pure 0.1 M $HClO_4$. The scan rate was 50 mV s^{-1}. Large-scale (30×30 nm^2) STM images of (c) C_{60}Fc directly attached on Au(111), acquired at 0.8 V vs RHE and (d) C_{60}Fc on the ZnOEP-modified Au(111), acquired at 0.8 V for (c) and 0.75 V vs RHE for (d) in 0.1 M $HClO_4$. Tip potentials and tunneling currents were 0.44 V and 5.3 nA for (a), and 0.46 V and 0.35 nA for (b), respectively. Reprinted with permission from Ref. 122, Copyright American Chemical Society (2004).

C_{60}Fc was attached on the ZnOEP-modified Au(111) surface. Based on redox potential of ferrocene moiety reported by several groups,[10–12] the CV profile drawn with a solid red line in Fig. 20b is associated with the electrochemical redox reaction of Fc to Fc^+ in each molecule of C_{60}Fc. From the electronic charge calculated from the oxidative peak area, the amount of electronic charge transferred was estimated to be ca. 8.0 μC cm^{-2}. If a one-electron redox reaction occurs on the C_{60}Fc/ZnOEP-modified Au(111) electrode, the value corresponds to the surface concentration of $(8.1 \pm 0.3) \times 10^{-11}$ mol cm^{-2}. The peak separation was almost immeasurable in Fig. 20b, indicating that the electron-transfer process is very rapid. This STM image of an adlayer of C_{60}Fc formed directly on a clean Au(111) showed a disordered structure, although individual molecules of C_{60}Fc could be discriminated as bright spots (see Fig. 20c). On the contrary, highly ordered arrays consisting of bright round spots were found on the ZnOEP-modified Au(111), as shown in Fig. 20d. Careful inspection revealed that each molecule has a dumbbell shape in the high-resolution STM image shown in Fig. 21a, suggesting that there is a difference in either electronic structure or molecular orientation of C_{60}Fc molecule. A structural model was the same as that of opened C_{60} (Fig. 21b). The CV and STM images suggest that the electrochemical response of Fc moiety is clearly enhanced on the highly ordered ZnOEP-modified Au(111) surface, but not on the unmodified Au(111) surface.

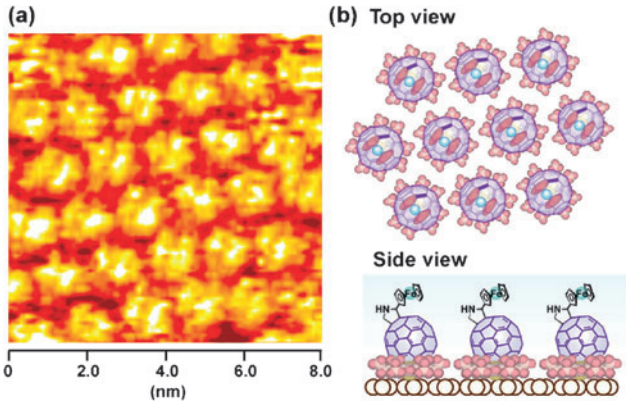

Fig. 21. (a) High-resolution STM image (8×8 nm^2) of the underlying layer of C_{60}Fc/ZnOEP supramolecular assembled layer on Au(111) in 0.1 M $HClO_4$ acquired at 0.75 V. Tip potential and tunneling current were 0.46 V and 1.8 nA, respectively. (b) Structural model for the C_{60}Fc/ZnOEP supramolecular assembled adlayer on Au(111). Reprinted with permission from Ref. 122, Copyright American Chemical Society (2004).

4.2 Effect of Central Metal Ions. To elucidate details of the effect of the central metal ion in OEP, we investigated OEPs with other metals such as CoOEP, CuOEP, and FeClOEP as an underlying adsorbed layer. Figure 22 shows CVs of C_{60}Fc on CoOEP-, CuOEP-, and FeClOEP-modified Au(111) electrodes. It is seen from (a) and (b) in Fig. 22 that the double-layer charging currents of CoOEP and CuOEP on Au(111) electrodes (dotted lines) were suppressed by the adsorption of C_{60}Fc molecule. Especially, Figure 22a shows that the reduction of Co(III) to Co(II) of CoOEP layer observed at 0.32 V disappeared, suggesting that the CoOEP layer was entirely covered with C_{60}Fc molecules. Judging from the oxidative peak area, we calculated the electronic charges consumed during the oxidation to be 6.1 and 4.8 μC cm^{-2} for CoOEP and CuOEP layers, respectively. The electronic charge of CuOEP consumed by the oxidation reaction of Fc to Fc^+ was estimated to be slightly lower than that of CoOEP. Furthermore, when FeClOEP was used as an underlying adsorbed layer, a clearly different CV was obtained. As shown in Fig. 22c, the redox peak currents observed at 0.79 V were much smaller than those of ZnOEP-, CoOEP-, and CuOEP-modified Au(111) electrodes, and another reductive peak appeared at 0.41 V corresponding to the reduction of Fe(III) to Fe(II) in FeClOEP. This result suggests that the surface was not fully covered with C_{60}Fc molecules.

To understand details of the interfacial phenomena, STM measurements were carried out in 0.1 M $HClO_4$ for each case.[122] Hexagonal molecular arrangements were clearly observed by the same procedure for three different metal-coordinated OEPs (see Figs. 22d–22f). Only one difference was found in STM image between CuOEP and CoOEP (or FeClOEP), i.e., the center spot of each CuOEP appeared as a dark spot, whereas that of CoOEP (or FeClOEP) was bright. This difference can be explained in terms of the difference in the mode of d_{z^2} orbital. Figures 22g–22i show typical STM images of the C_{60}Fc arrays formed on CoOEP-, CuOEP-, and FeClOEP-modified Au(111) surfaces, respectively. As can be seen in Figs. 22g and 22h,

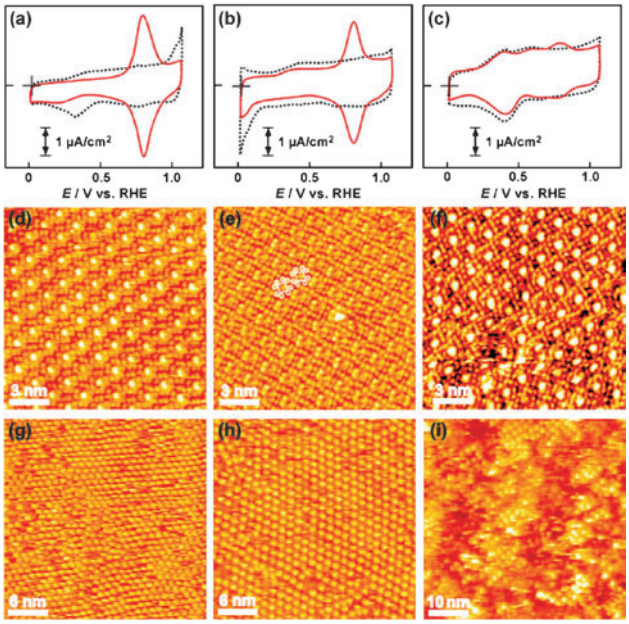

Fig. 22. Cyclic voltammograms recorded at scan rate of 50 mV s^{-1} of C_{60}Fc on (a) CoOEP-, (b) CuOEP-, and (c) FeClOEP-modified Au(111) (red solid line) in pure 0.1 M $HClO_4$. The dotted lines show voltammograms of the underlying MOEP-modified Au(111) electrode. High-resolution STM images (15×15 nm^2) of (d) CoOEP, (e) CuOEP, and (f) FeClOEP underlying layers on Au(111) surface, and large-scale STM images of C_{60}Fc arrays on (g) CoOEP-, (h) CuOEP-, and (i) FeClOEP-modified Au(111) acquired at 0.75 V vs RHE in 0.1 M $HClO_4$. Tip potentials and tunneling currents were 0.46 V and 0.35 nA for (g), 0.46 V and 0.36 nA for (h) and 0.46 V and 0.38 nA for (i), respectively. Reprinted with permission from Ref. 122, Copyright American Chemical Society (2004).

C_{60}Fc molecules were hexagonally arranged. Adlattices of C_{60}Fc on the CoOEP and CuOEP adlayers were almost identical to that on the ZnOEP adlayer. The STM images shown in Figs. 22g and 22h indicated that C_{60}Fc molecules entirely covered both surfaces. The difference in the electronic charge found on the CVs in Figs. 22a and 22b might be due to the difference in electronic state of central metal ion between Co(II) and Cu(II) ions. These results suggest that the central metal ions significantly affect the electron-transfer reaction between Fc moiety in C_{60}Fc and MOEP molecules. Such metal ion dependence was reported in the investigation on affinity between metalloporphyrin cyclic dimer and fullerene. According to a paper by Aida et al., the association constants, K_{assoc} values for metalloporphyrin cyclic dimer of Co and Zn ions were greater than 10^7 M^{-1}, whereas the other three host molecules with other metal ions such as Ni, Cu, and Ag were inferior to the above host molecules ($K_{assoc} < 10^7$ M^{-1}).[133] Furthermore, recent DFT calculations for supramolecular interactions between metalloporphyrin and C_{60} showed that the interaction energy is strongly influenced by central metal ions.[127] Figure 22i shows a typical large-scale STM image of C_{60}Fc array on the FeClOEP-modified Au(111) surface. The scan area was 50×50 nm^2. Although some ordered areas are visible, the entire surface was rough. After the potential was modulated to values more negative than 0.4 V, a disordered structure of C_{60}Fc appeared on the surface. This is attributed to the mobility of underlying FeClOEP molecules. As described in our recent paper, FeClOEP molecules are highly mobile due to the reduction of central iron(III) to iron(II) at potentials more negative than 0.4 V,[112] although FeClOEP molecules also formed a hexagonally packed adlayer similar to adlayers of ZnOEP, CoOEP, and CuOEP. Thus, the coordination of Cl is likely to affect significantly the fullerene and porphyrin supramolecular assembly on metal surfaces. Note that electrochemical response of Fc moiety was also poorly at carbon monoxide-coordinated Ru(III)OEP (Ru(CO)OEP)-modified Au(111) electrode.[134] The effect of central metal ion in OEP on the formation of supramolecular assemblies with C_{60}Fc molecule was clearly demonstrated. The same tendency was also found at supramolecular-assembled layers with opened C_{60}.[134]

5. Summary and Outlook

In this article, to elucidate and to understand surface functionalities of various organic molecules at electrochemical interfaces, it was described on the relationship between surface function and adlayer structure for cytochrome *c* electrochemistry, electrochemical reduction of O_2 on porphyrin adlayers, and molecular orientation controlled by the formation of supramolecular assembly at electrochemical interfaces by using STM. The results obtained in this research are summarized below.

(1) A 4-PyS-modified Au(111) electrode gave a well-defined voltammetric response of cytochrome *c*, whereas no electrochemical responses of cytochrome *c* were observed at 2-PyS-modified Au(111) single-crystal electrode. In situ STM observation clearly revealed that Py moiety of 4-PyS faced to solution while 2-PyS adsorbs through both thiolate S and pyridine N atoms on both Au(111) and Au(100) surfaces. The pyridine N atoms facing to the solution are a key factor and surface functionality of promoter molecules for the rapid electron transfer of cytochrome *c* was clarified at molecular level.

(2) CoPor- or CoPc-modified Au(111) electrode studies indicated that the two-electron reduction process of O_2 to H_2O_2 proceeded on the CoP-, CoOEP-, CoTPP-, and CoPc-modified Au(111) surfaces, whereas FeClOEP indicated two-step four-electron reduction of O_2 to H_2O. From the results of in situ STM, we concluded the stability of adlayers on the electrode surface is one of important factors controlling the electrochemical activity for the reduction of O_2. Furthermore, binary molecular arrays consisting of Pc and Por were controlled by potential modulation and crystallographic orientation of Au.

(3) Molecular orientation and the electrochemical reaction of redox-active moieties can be controlled by using a simple method for the construction of a 1:1 supramolecular-assembled film. In addition, it was suggested that precise control of underlying ZnOEP adlayers with Au atomic structure is important to recognize fullerenes. The unique approach was established as a new modification method.

Thus, molecular assemblies and molecular orientations of functional organic molecules at electrode surfaces were elucidated and understood in aqueous solutions by using electro-

chemical STM at molecular level with electrochemical properties. Our results demonstrated that electrode potential modulation and control of crystallographic orientations play significant roles in the precise control of two-dimensional supramolecular nanoarchitectures.

As mentioned in this article, the understanding for the interactions between both intermolecular and molecules-substrate in two-dimensionally self-organized films at molecular level both in UHV and in solution has considerably progressed by STM techniques in the past decade, and the results have provided the knowledge for new surface design and patterning. Especially, the control and design of characteristic molecular assemblies using non-covalent intermolecular interactions, such as dipole–dipole interaction, hydrogen bonding, electrostatic interaction, metal–ligand coordination, and π–π interaction on surfaces, is a most promising approach for construction of nanoarchitectures. Such "bottom-up" strategy based on supramolecular chemistry makes it possible to create desired supramolecular crystals or complex from solution phase. In recent years, metal–ligand coordination has been extensively investigated by many organic chemists.[38,39,135–140] The key to coordination-based self-assembly is the ability to manipulate the process of molecular recognition and to generate an enormous variety of rigid framework assemblies featuring well-defined nano-scale cavities. This is a considerable promising approach for the recognition and binding phase of small molecule sensing.[141,142] However, it is not so easy to directly apply the knowledge of supramolecular chemistry to surfaces. The concepts of solution-based supramolecular chemistry would be appropriately modified to extend supramolecular assembly technique onto substrate. One of attractive approaches for the modification is direct building up of nanoarchitectures by metal–organic coordination on surfaces. Construction and control of various 2D metallosupramolecular surface structures, such as chirality, nano cavity, and network arrays have been attempted in UHV.[143] For example, surface-supported Fe–carboxylate coordination with controlled cavity size and functionality represent robust templates for the handling and organization of functional species at nanoscale. An effective idea for adjusting the size of the cavities is provided by careful selection of suitable linker compounds with deposition of appropriate metals as a glue. The tuning of lateral interaction is particularly important for selective adsorption of guest molecules. Electrochemical control of supramolecular assemblies might also be a promising method.[34,35,115,116a,144] In the future, not only two-dimensionally but also three-dimensionally self-organized growth of functional molecules at surfaces can be produced by skillfully utilizing the knowledge of supramolecular assembly combined with chemical and biological bottom-up techniques.

The author would like to express his sincerest thanks to Prof. Kingo Itaya (Tohoku University) for his invaluable comments and suggestions. The author acknowledges Prof. Koichi Komatsu (Institute for Chemical Research, Kyoto University), Prof. Osamu Ito (Institute of Institute of Multidisciplinary Research for Advanced Materials, Tohoku University), Prof. Francis D'Souza (Department of Chemistry, Wichita State University), Prof. Nagao Kobayashi (Graduate School of Science, Department of Chemistry, Tohoku University), and Prof. Hiroyuki Furuta (Graduate school of Engineering, Kyushu University), for their collaborations. The author would like to express appreciation to Prof. Isao Taniguchi (Kumamoto University) for his constant encouragement. This work was supported in part by Core Research Evolutional Science and Technology organized by Japan Science and Technology Agency (CREST-JST), and by the Ministry of Education, Culture, Sports, Science and Technology, a Grant-in-Aid for Young Scientists (B) (No. 16750106) and the Center of Excellence (COE) Project, Giant Molecules and Complex Systems, 2005.

References

1 a) I. Taniguchi, *Interfacial Electrochemistry of Promoter Modified Electrodes for the Rapid Electron Transfer of Cytochrome c*, in *Redox Chemistry and Interfacial Behavior of Biological Molecules*, ed. by G. Dryhurst, Plenum Press, New York, **1988**, p. 113. b) I. Taniguchi, in *Redox Mechanisms and Interfacial Properties of Molecules of Biological Importance*, ed. by F. A. Schultz, I. Taniguchi, Electrochemical Soc., Inc., Pennington, **1993**, p. 9. c) I. Taniguchi, F. M. Hawkridge, *Comments Inorg. Chem.* **1995**, *17*, 163. d) I. Taniguchi, S. Yoshimoto, M. Yoshida, Y. Mie, K. Kudo, K. Nishiyama, in *Novel Trends in Electroorganic Synthesis*, ed. by S. Torii, Springer-Verlag, Tokyo, **1998**, p. 175.

2 a) I. Taniguchi, K. Toyosawa, H. Yamaguchi, K. Yasukouchi, *J. Chem. Soc., Chem. Commun.* **1982**, 1032. b) I. Taniguchi, K. Toyosawa, H. Yamaguchi, K. Yasukouchi, *J. Electroanal. Chem.* **1982**, *140*, 187.

3 a) I. Taniguchi, M. Iseki, K. Toyosawa, H. Yamaguchi, K. Yasukouchi, *J. Electroanal. Chem.* **1984**, *164*, 385. b) I. Taniguchi, T. Funatsu, M. Iseki, H. Yamaguchi, K. Yasukouchi, *J. Electroanal. Chem.* **1985**, *193*, 295. c) I. Taniguchi, H. Kurihara, K. Yoshida, M. Tominaga, F. M. Hawkridge, *Denki Kagaku* **1992**, *60*, 1043. d) M. Tominaga, K. Hayashi, I. Taniguchi, *Anal. Sci.* **1992**, *8*, 829.

4 a) I. Taniguchi, K. Watanabe, M. Tominaga, F. M. Hawkridge, *J. Electroanal. Chem.* **1992**, *333*, 331. b) M. Tominaga, T. Kumagai, S. Takita, I. Taniguchi, *Chem. Lett.* **1993**, 1771.

5 a) I. Taniguchi, Y. Hirakawa, K. Iwakiri, M. Tominaga, K. Nishiyama, *J. Chem. Soc., Chem. Commun.* **1994**, 953. b) I. Taniguchi, R. Muraguchi, K. Nishiyama, *Denki Kagaku* **1994**, *62*, 985. c) K. Nishiyama, H. Ishida, I. Taniguchi, *J. Electroanal. Chem.* **1994**, *373*, 255.

6 a) *Introduction to Ultrathin Organic Films*, ed. by A. Ulman, Academic Press, Boston, **1991**. b) A. Ulman, *Chem. Rev.* **1996**, *96*, 1533. c) *Thin Films: Self-Assembled Monolayers of Thiols*, ed. by A. Ulman, Academic Press, San Diego, **1998**. d) A. Ulman, *Acc. Chem. Res.* **2001**, *34*, 855.

7 a) J. C. Love, L. A. Estroff, J. K. Kriebel, R. G. Nuzzo, G. M. Whitesides, *Chem. Rev.* **2005**, *105*, 1103. b) B. D. Gates, Q. Xu, M. Stewart, D. Ryan, C. G. Willson, G. M. Whitesides, *Chem. Rev.* **2005**, *105*, 1171.

8 G. E. Poirier, *Chem. Rev.* **1997**, *97*, 1117, and references therein.

9 a) H. Imahori, K. Tamaki, Y. Araki, Y. Sekiguchi, O. Ito, Y. Sakata, S. Fukuzumi, *J. Am. Chem. Soc.* **2002**, *124*, 5165. b) T. J. Kesti, N. V. Tkachenko, V. Vehmanen, H. Yamada, H. Imahori, S. Fukuzumi, H. Lemmetyinen, *J. Am. Chem. Soc.* **2002**, *124*, 8067. c) H. Yamada, H. Imahori, Y. Nishimura, I.

Yamazaki, T. K. Ahn, S.-K. Kim, D. Kim, S. Fukuzumi, *J. Am. Chem. Soc.* **2003**, *125*, 9129. d) H. Imahori, S. Fukuzumi, *Adv. Funct. Mater.* **2004**, *14*, 525.

10 a) M. D. Porter, J. B. Bright, D. L. Allara, C. E. D. Chidsey, *J. Am. Chem. Soc.* **1987**, *109*, 3559. b) C. E. D. Chidsey, C. R. Bertozzi, T. M. Putvinski, A. M. Mujsce, *J. Am. Chem. Soc.* **1990**, *112*, 4301. c) C. E. D. Chidsey, *Science* **1991**, *251*, 919. d) D. D. Popenoe, R. S. Deinhammer, M. D. Porter, *Langmuir* **1992**, *8*, 2521.

11 a) K. Uosaki, Y. Sato, H. Kita, *Langmuir* **1991**, *7*, 1510. b) K. Shimazu, I. Yagi, Y. Sato, K. Uosaki, *Langmuir* **1992**, *8*, 1385. c) K. Shimazu, S. Ye, Y. Sato, K. Uosaki, *J. Electroanal. Chem.* **1994**, *375*, 409. d) S. Ye, Y. Sato, K. Uosaki, *Langmuir* **1997**, *13*, 3157.

12 K. Nishiyama, A. Ueda, S. Tanoue, T. Koga, I. Taniguchi, *Chem. Lett.* **2000**, 930.

13 a) P. M. Allen, H. A. O. Hill, N. J. Walton, *J. Electroanal. Chem.* **1984**, *178*, 69. b) H. A. O. Hill, D. J. Page, N. J. Walton, D. Whitford, *J. Electroanal. Chem.* **1985**, *187*, 315. c) K. D. Gleria, H. A. O. Hill, V. J. Lowe, D. J. Page, *J. Electroanal. Chem.* **1986**, *213*, 333. d) F. A. Armstrong, H. A. O. Hill, N. J. Walton, *Acc. Chem. Res.* **1988**, *21*, 407.

14 a) M. J. Tarlov, E. F. Bowden, *J. Am. Chem. Soc.* **1991**, *113*, 1847. b) S. Dong, R. A. Clarrk, E. F. Bowden, M. J. Tarlov, *J. Phys. Chem.* **1993**, *97*, 6564. c) J. D. H. Glenn, E. F. Bowden, *Chem. Lett.* **1996**, 399.

15 C. Zhou, S. Ye, T. M. Cotton, X. Yu, T. Lu, S. Dong, *J. Electroanal. Chem.* **1991**, *319*, 71.

16 a) Y. Sato, F. Mizutani, *J. Electroanal. Chem.* **1999**, *473*, 99. b) Y. Sato, F. Mizutani, *Electrochim. Acta* **2000**, *45*, 2869.

17 a) J. P. Collman, R. R. Gagne, T. R. Halbert, J. C. Marchon, C. A. Reed, *J. Am. Chem. Soc.* **1973**, *95*, 7868. b) J. P. Collman, R. R. Gagne, C. A. Reed, T. R. Halbert, G. Lang, W. T. Robinson, *J. Am. Chem. Soc.* **1975**, *97*, 1427. c) J. P. Collman, R. Boulatov, C. J. Sunderland, L. Fu, *Chem. Rev.* **2004**, *104*, 561.

18 a) J. P. Collman, M. Marrocco, P. Denisevich, Y. Konai, C. Koval, F. C. Anson, *J. Electroanal. Chem. Interfacial Electrochem.* **1979**, *101*, 117. b) J. P. Collman, P. Denisevich, Y. Konai, M. Marrocco, C. Koval, F. C. Anson, *J. Am. Chem. Soc.* **1980**, *102*, 6027. c) J. P. Collman, P. S. Wagenknecht, J. E. Hutchison, *Angew. Chem., Int. Ed. Engl.* **1994**, *33*, 1537, and references therein.

19 a) J. Zagal, R. K. Sen, E. Yeager, *J. Electroanal. Chem. Interfacial Electrochem.* **1977**, *83*, 207. b) E. Yeager, *Electrochim. Acta* **1984**, *29*, 1527, and references therein.

20 a) K. Shigehara, F. C. Anson, *J. Phys. Chem.* **1982**, *86*, 2776. b) C. Shi, B. Steiger, M. Yuasa, F. C. Anson, *Inorg. Chem.* **1997**, *36*, 4294. c) E. Song, C. Shi, F. C. Anson, *Langmuir* **1998**, *14*, 4315. d) C. Shi, F. C. Anson, *Inorg. Chem.* **1998**, *37*, 1037. e) F. C. Anson, C. Shi, A. Steiger, *Acc. Chem. Res.* **1997**, *30*, 437.

21 a) *Electron Transfer in Chemistry*, ed. by V. Balzani, Wiley-VCH, New York, **2001**, Vol. 3. b) S. Fukuzumi, *Org. Biomol. Chem.* **2003**, *1*, 609. c) H. Imahori, Y. Mori, Y. Matano, *J. Photochem. Photobiol., C* **2003**, *4*, 51. d) H. Imahori, *Org. Biomol. Chem.* **2004**, *2*, 1425.

22 H. Imahori, K. Hagiwara, M. Aoki, T. Akiyama, S. Taniguchi, T. Okada, M. Shirakawa, Y. Sakata, *J. Am. Chem. Soc.* **1996**, *118*, 11771.

23 D. Kuciauskas, S. Lin, G. R. Seely, A. L. Moore, T. A. Moore, D. Gust, T. Drovetskaya, C. A. Reed, P. D. W. Boyd, *J. Phys. Chem.* **1996**, *100*, 15926.

24 K. Tashiro, T. Aida, J.-Y. Zheng, K. Kinbara, K. Saigo, S. Sakamoto, K. Yamaguchi, *J. Am. Chem. Soc.* **1999**, *121*, 9477.

25 D. Sun, F. S. Tham, C. A. Reed, L. Chaker, M. Burgess, D. W. Boyd, *J. Am. Chem. Soc.* **2000**, *122*, 10704.

26 D. Gust, T. A. Moore, A. L. Moore, *Acc. Chem. Res.* **2001**, *34*, 40.

27 D. M. Guldi, *Chem. Soc. Rev.* **2002**, *31*, 22.

28 M. E. El-Khouly, O. Ito, P. M. Smith, F. D'Souza, *J. Photochem. Photobiol., C* **2004**, *5*, 79.

29 a) T. Da Ros, M. Prato, D. M. Guldi, M. Ruzzi, L. Pasimeni, *Chem. Eur. J.* **2001**, *7*, 816. b) D. I. Schuster, P. Cheng, P. D. Jarowski, D. M. Guldi, *J. Am. Chem. Soc.* **2004**, *126*, 7257.

30 P. D. W. Boyd, C. A. Reed, *Acc. Chem. Res.* **2005**, *38*, 235.

31 a) T. Yokoyama, S. Yokoyama, T. Kamikado, Y. Okuno, S. Mashiko, *Nature* **2001**, *413*, 619. b) T. Yokoyama, T. Kamikado, S. Yokoyama, S. Mashiko, *J. Chem. Phys.* **2004**, *121*, 11993.

32 Y.-G. Kim, S.-L. Yau, K. Itaya, *Langmuir* **1999**, *15*, 7810.

33 a) S. Griessl, M. Lackinger, M. Edelwirth, M. Hietschold, W. M. Heckl, *Single Mol.* **2002**, *3*, 25. b) S. J. H. Griessl, M. Lackinger, F. Jamitzky, T. Markert, M. Hietschold, W. M. Heckl, *Langmuir* **2004**, *20*, 9403. c) S. J. H. Griessl, M. Lackinger, F. Jamitzky, T. Markert, M. Hietschold, W. M. Heckl, *J. Phys. Chem. B* **2004**, *108*, 11556.

34 Y. Ishikawa, A. Ohira, M. Sakata, C. Hirayama, M. Kunitake, *Chem. Commun.* **2002**, 2652.

35 a) G.-J. Su, H.-M. Zhang, L.-J. Wan, C.-L. Bai, T. Wandlowski, *J. Phys. Chem. B* **2004**, *108*, 1931. b) Z. Li, B. Han, L.-J. Wan, T. Wandlowski, *Langmuir* **2005**, *21*, 6915.

36 A. Dmitriev, N. Lin, J. Weckesser, J. V. Barth, K. Kern, *J. Phys. Chem. B* **2002**, *106*, 6907.

37 S. De Feyter, F. C. De Schryver, *J. Phys. Chem. B* **2005**, *109*, 4290, and references therein.

38 a) J. A. A. W. Elemans, M. C. Lensen, J. W. Gerritsen, H. Kerpen, S. Speller, R. J. M. Nolte, A. E. Rowan, *Adv. Mater.* **2003**, *15*, 2070. b) M. C. Lensen, S. J. T. van Dingenen, J. A. A. W. Elemans, H. P. Dijkstra, G. P. M. van Klink, G. van Koten, J. W. Gerritsen, S. Speller, R. J. M. Nolte, A. E. Rowan, *Chem. Commun.* **2004**, 762.

39 O. Shoji, H. Tanaka, T. Kawai, Y. Kobuke, *J. Am. Chem. Soc.* **2005**, *127*, 8598.

40 S. Chiang, *Chem. Rev.* **1997**, *97*, 1083.

41 S. De Feyter, F. C. De Schryver, *Chem. Soc. Rev.* **2003**, *32*, 139.

42 A. A. Gewirth, B. K. Niece, *Chem. Rev.* **1997**, *97*, 1129.

43 K. Itaya, *Prog. Surf. Sci.* **1998**, *58*, 121, and references therein.

44 *Interfacial Electrochemistry*, ed. by A. Wieckowski, Marcel Dekker, New York, **1999**.

45 D. M. Kolb, *Angew. Chem., Int. Ed.* **2001**, *40*, 1162.

46 O. M. Magnussen, *Chem. Rev.* **2002**, *102*, 672.

47 W. Mamdouh, H. Ujii, A. E. Dulcey, V. Percec, S. De Feyter, F. C. De Schryver, *Langmuir* **2004**, *20*, 7678.

48 M. Lackinger, S. Griessl, W. M. Heckl, M. Hietschold, G. W. Flynn, *Langmuir* **2005**, *21*, 4984.

49 B. J. Gyarfas, B. Wiggins, M. Zosel, K. W. Hipps, *Langmuir* **2005**, *21*, 919.

50 a) S. Yoshimoto, R. Narita, K. Itaya, *Chem. Lett.* **2002**, 356. b) S. Yoshimoto, R. Narita, M. Wakisaka, K. Itaya, *J. Electroanal. Chem.* **2002**, *532*, 331.

51 a) S. Yoshimoto, R. Narita, E. Tsutsumi, M. Matsumoto, K. Itaya, O. Ito, K. Fujiwara, Y. Murata, K. Komatsu, *Langmuir* **2002**, *18*, 8518. b) M. Matsumoto, J. Inukai, E. Tsutsumi, S.

Yoshimoto, K. Itaya, O. Ito, K. Fujiwara, M. Murata, Y. Murata, K. Komatsu, *Langmuir* **2004**, *20*, 1245.

52 J. Clavilier, R. Faure, G. Guinet, R. Durand, *J. Electroanal. Chem.* **1980**, *107*, 205.

53 a) A. Hamelin, in *Modern Aspects of Electrochemistry*, ed. by B. E. Conway, R. E. White, J. O'M. Bockris, Plenum Press, New York, **1985**, No. 16, Chap. 1. b) H. Angerstein-Kozlowska, B. E. Conway, A. Hamelin, L. Stoicoviciu, *Electrochim. Acta* **1986**, *31*, 1051. c) H. Angerstein-Kozlowska, B. E. Conway, A. Hamelin, L. Stoicoviciu, *J. Electroanal. Chem.* **1987**, *228*, 429. d) A. Hamelin, *J. Electroanal. Chem.* **1996**, *407*, 1.

54 D. A. Scherson, D. M. Kolb, *J. Electroanal. Chem.* **1984**, *176*, 353.

55 a) A. S. Dakkouri, D. M. Kolb, in *Interfacial Electrochemistry*, ed. by A. Wieckowski, Marcel Dekker, New York, **1999**, Chap. 10. b) A. Cuesta, M. Kleinert, D. M. Kolb, *Phys. Chem. Chem. Phys.* **2000**, *2*, 5684.

56 O. M. Magnussen, J. Hageböck, J. Hotlos, R. J. Bhem, *Faraday Discuss.* **1992**, *94*, 329.

57 G. J. Edens, X. Gao, M. J. Weaver, *J. Electroanal. Chem.* **1994**, *375*, 357.

58 a) A. M. Funtikov, U. Linke, U. Stimming, R. Vogel, *Surf. Sci.* **1995**, *324*, L343. b) A. M. Funtikov, U. Stimming, R. Vogel, *J. Electroanal. Chem.* **1997**, *428*, 147.

59 L.-J. Wan, S.-L. Yau, K. Itaya, *J. Phys. Chem.* **1995**, *99*, 9507.

60 L.-J. Wan, M. Hara, J. Inukai, K. Itaya, *J. Phys. Chem. B* **1999**, *103*, 6978.

61 a) L.-J. Wan, T. Suzuki, K. Sashikata, J. Okada, J. Inukai, K. Itaya, *J. Electroanal. Chem.* **2000**, *484*, 189. b) J. Okada, J. Inukai, K. Itaya, *Phys. Chem. Chem. Phys.* **2001**, *3*, 3297.

62 a) M. Wilms, P. Broekmann, M. Kruft, Z. Park, C. Stuhlmann, K. Wandelt, *Surf. Sci.* **1998**, *402–404*, 83. b) M. Wilms, P. Broekmann, C. Stuhlmann, K. Wandelt, *Surf. Sci.* **1998**, *416*, 121. c) M. Lennartz, P. Broekmann, M. Arenz, C. Stuhlmann, K. Wandelt, *Surf. Sci.* **1999**, *442*, 215.

63 K. Sato, S. Yoshimoto, J. Inukai, K. Itaya, *Electrochem. Commun.* **2006**, *8*, 725.

64 a) I. Taniguchi, *Denki Kagaku* **1988**, *56*, 158. b) I. Taniguchi, *Seibutsu Butsuri* **1994**, *34*, 72.

65 I. Taniguchi, S. Yoshimoto, K. Nishiyama, *Chem. Lett.* **1997**, 353.

66 T. Sawaguchi, F. Mizutani, S. Yoshimoto, I. Taniguchi, *Electrochim. Acta* **2000**, *45*, 2861.

67 a) S. Yoshimoto, M. Yoshida, S. Kobayashi, S. Nozute, T. Miyawaki, Y. Hashimoto, I. Taniguchi, *J. Electroanal. Chem.* **1999**, *473*, 85. b) I. Taniguchi, S. Yoshimoto, M. Yoshida, S.-i. Kobayashi, T. Miyawaki, Y. Aono, Y. Sunatsuki, H. Taira, *Electrochim. Acta* **2000**, *45*, 2843.

68 *Surface Electrochemistry—A Molecular Approach—*, ed. by J. O'M. Bockris, S. U. M. Khan, Plenum Press, New York, **1993**, Chap. 7, pp. 663–744.

69 M. A. Bryant, R. M. Crooks, *Langmuir* **1993**, *9*, 385.

70 I. Taniguchi, S. Yoshimoto, Y. Sunatsuki, K. Nishiyama, *Electrochemistry* **1999**, *67*, 1197.

71 T. Sawaguchi, I. Taniguchi, F. Mizutani, *Langmuir* **1998**, *14*, 3565.

72 a) C. A. Widrig, C. A. Alves, M. D. Porter, *J. Am. Chem. Soc*. **1991**, *113*, 2805. b) C. A. Widrig, C. Chung, M. D. Porter, *J. Electroanal. Chem.* **1991**, *310*, 335.

73 L.-J. Wan, Y. Hara, H. Noda, M. Osawa, *J. Phys. Chem. B* **1998**, *102*, 5943.

74 Q. Jin, J. A. Rodriguez, C. Z. Li, Y. Darici, N.-J. Tao, *Surf. Sci.* **1999**, *425*, 101.

75 T. Baunach, V. Ivanova, D. A. Scherson, D. M. Kolb, *Langmuir* **2004**, *20*, 2797.

76 W. Zhou, T. Baunach, V. Ivanova, D. M. Kolb, *Langmuir* **2004**, *20*, 4590.

77 T. Sawaguchi, F. Mizutani, I. Taniguchi, *Anal. Sci.* **2001**, *17*, Suppl., i383.

78 T. Sawaguchi, S. Yoshimoto, F. Mizutani, I. Taniguchi, unpublished results.

79 I. Taniguchi, H. Ishimoto, K. Miyagawa, M. Iwai, H. Nagai, H. Hanazono, K. Taira, A. Kubo, A. Nishikawa, K. Nishiyama, Z. Dursun, G. P.-J. Hareau, M. Tazaki, *Electrochem. Commun.* **2003**, *5*, 857.

80 a) T. Sawaguchi, Y. Sato, F. Mizutani, *J. Electroanal. Chem.* **2001**, *496*, 50. b) T. Sawaguchi, Y. Sato, F. Mizutani, *J. Electroanal. Chem.* **2001**, *507*, 256. c) T. Sawaguchi, Y. Sato, F. Mizutani, *Phys. Chem. Chem. Phys.* **2001**, *3*, 3399.

81 T. Sawaguchi, Y. Sato, F. Mizutani, *Electrochemistry* **2001**, *69*, 962.

82 L.-J. Wan, M. Terashima, H. Noda, M. Osawa, *J. Phys. Chem. B* **2000**, *104*, 3563.

83 S. Yoshimoto, T. Sawaguchi, F. Mizutani, I. Taniguchi, *Electrochem. Commun.* **2000**, *2*, 39.

84 S. Yoshimoto, T. Sawaguchi, F. Mizutani, I. Taniguchi, unpublished results.

85 a) *Calixarenes Revisited*, ed. by C. D. Gutsche, The Royal Society of Chemistry, Cambridge, **1998**. b) W. Hill, B. Wehling, C. G. Gibbs, C. D. Gutsche, D. Klockow, *Anal. Chem.* **1995**, *67*, 3187. c) M. T. Cygan, G. E. Collins, T. D. Dunbar, D. L. Allara, C. G. Gibbs, C. D. Gutsche, *Anal. Chem.* **1999**, *71*, 142.

86 A. Ikeda, S. Shinkai, *Chem. Rev.* **1997**, *97*, 1713.

87 K. Nakano, S. Tanaka, M. Takagi, S. Shinkai, *Chem. Lett.* **2000**, 60.

88 a) S.-K. Kang, T.-D. Chung, H. Kim, *Electrochim. Acta* **2000**, *45*, 2939. b) J. Park, S.-K. Kang, T.-D. Chung, S.-K. Chang, H. Kim, *Microchem. J.* **2001**, *68*, 109. c) T.-D. Chung, J. Park, J. Kim, H. Lim, M.-J. Choi, J. R. Kim, S.-K. Chang, H. Kim, *Anal. Chem.* **2001**, *68*, 3975.

89 a) H. Schönherr, G. J. Vancso, B.-H. Huisman, F. C. J. M. van Veggel, D. N. Reinhoudt, *Langmuir* **1999**, *15*, 5541. b) H. Schönherr, G. J. Vancso, B.-H. Huisman, F. C. J. M. van Veggel, D. N. Reinhoudt, *Langmuir* **1997**, *13*, 1567.

90 S. Raible, J. Pfeiffer, T. Weiss, W. Clauss, W. Goepel, V. Schurig, D. P. Kern, *Appl. Phys. A* **2000**, *70*, 607.

91 T. Sakai, A. Ohira, M. Sakata, C. Hirayama, M. Kunitake, *Chem. Lett.* **2001**, 782.

92 G.-B. Pan, L.-J. Wan, Q.-Y. Zheng, C.-L. Bai, K. Itaya, *Chem. Phys. Lett.* **2002**, *359*, 83.

93 a) C. G. Gibbs, C. D. Gutsche, *J. Am. Chem. Soc.* **1993**, *115*, 5338. b) C. G. Gibbs, P. K. Sujeeth, J. S. Rogers, G. G. Stanley, M. Krawiec, W. H. Watson, C. D. Gutsche, *J. Org. Chem.* **1995**, *60*, 8394.

94 X. Delaigue, M. W. Hosseini, N. Kyritsakas, A. De Cian, J. Fischer, *J. Chem. Soc., Chem. Commun.* **1995**, 609.

95 S. Yoshimoto, M. Abe, K. Itaya, F. Narumi, K. Sashikata, K. Nishiyama, I. Taniguchi, *Langmuir* **2003**, *19*, 8130.

96 S. Yoshimoto, N. Hirakawa, K. Nishiyama, I. Taniguchi, *Langmuir* **2000**, *16*, 4399.

97 a) T. Kuwana, M. Fujihira, K. Sunakawa, T. Osa, *J. Electroanal. Chem.* **1978**, *88*, 299. b) N. Kobayashi, T. Matsue, M. Fujihira, T. Osa, *J. Electroanal. Chem.* **1979**, *103*, 427.

98 P. A. Forshey, T. Kuwana, *Inorg. Chem.* **1983**, *22*, 699.
99 P. H. Lippel, R. J. Wilson, M. D. Miller, C. Wöll, S. Chiang, *Phys. Rev. Lett.* **1989**, *62*, 171.
100 a) T. A. Jung, R. R. Schlittler, J. K. Gimzewski, H. Tang, C. Joachim, *Science* **1996**, *271*, 181. b) T. A. Jung, R. R. Schlittler, J. K. Gimzewski, *Nature* **1997**, *386*, 696.
101 a) X. Lu, K. W. Hipps, X. D. Wang, U. Mazur, *J. Am. Chem. Soc.* **1996**, *118*, 7197. b) K. W. Hipps, X. Lu, X. D. Wang, U. Mazur, *J. Phys. Chem.* **1996**, *100*, 11207. c) X. Lu, K. W. Hipps, *J. Phys. Chem. B* **1997**, *101*, 5391.
102 I. Chizhov, G. Scoles, A. Kahn, *Langmuir* **2000**, *16*, 4358.
103 a) L. Scudiero, D. E. Barlow, K. W. Hipps, *J. Phys. Chem. B* **2000**, *104*, 11899. b) L. Scudiero, D. E. Barlow, U. Mazur, K. W. Hipps, *J. Am. Chem. Soc.* **2001**, *123*, 4073. c) L. Scudiero, D. E. Barlow, K. W. Hipps, *J. Phys. Chem. B* **2002**, *106*, 996.
104 a) K. W. Hipps, L. Scudiero, D. E. Barlow, M. P. Cooke, Jr., *J. Am. Chem. Soc.* **2002**, *124*, 2126. b) L. Scudiero, K. W. Hipps, D. E. Barlow, *J. Phys. Chem. B* **2003**, *107*, 2903. c) D. E. Barlow, L. Scudiero, K. W. Hipps, *Langmuir* **2004**, *20*, 4413.
105 a) M. Kunitake, N. Batina, K. Itaya, *Langmuir* **1995**, *11*, 2337. b) N. Batina, M. Kunitake, K. Itaya, *J. Electroanal. Chem.* **1996**, *405*, 245. c) M. Kunitake, U. Akiba, N. Batina, K. Itaya, *Langmuir* **1997**, *13*, 1607.
106 K. Ogaki, N. Batina, M. Kunitake, K. Itaya, *J. Phys. Chem.* **1996**, *100*, 7185.
107 K. Sashikata, T. Sugata, M. Sugimasa, K. Itaya, *Langmuir* **1998**, *14*, 2896.
108 L.-J. Wan, S. Shundo, J. Inukai, K. Itaya, *Langmuir* **2000**, *16*, 2164.
109 Y. He, T. Ye, E. Borguet, *J. Am. Chem. Soc.* **2002**, *124*, 11964.
110 a) N.-J. Tao, G. Cardenas, F. Cunha, Z. Shi, *Langmuir* **1995**, *11*, 4445. b) N.-J. Tao, *Phys. Rev. Lett.* **1996**, *76*, 4066.
111 a) S. Yoshimoto, J. Inukai, A. Tada, T. Abe, T. Morimoto, A. Osuka, H. Furuta, K. Itaya, *J. Phys. Chem. B* **2004**, *108*, 1948. b) S. Yoshimoto, A. Tada, K. Suto, R. Narita, K. Itaya, *Langmuir* **2003**, *19*, 672. c) S. Yoshimoto, A. Tada, K. Suto, K. Itaya, *J. Phys. Chem. B* **2003**, *107*, 5836.
112 S. Yoshimoto, A. Tada, K. Itaya, *J. Phys. Chem. B* **2004**, *108*, 5171.
113 a) S. Yoshimoto, K. Suto, K. Itaya, N. Kobayashi, *Chem. Commun.* **2003**, 2174. b) S. Yoshimoto, K. Suto, A. Tada, N. Kobayashi, K. Itaya, *J. Am. Chem. Soc.* **2004**, *126*, 8020.
114 a) N. Kobayashi, Y. Nishiyama, *J. Chem. Soc., Chem. Commun.* **1986**, 1462. b) N. Kobayashi, A. B. P. Lever, *J. Am. Chem. Soc.* **1987**, *109*, 7433. c) N. Kobayashi, *Coord. Chem. Rev.* **2002**, *227*, 129.
115 S. Yoshimoto, N. Yokoo, T. Fukuda, N. Kobayashi, K. Itaya, *Chem. Commun.* **2006**, 500.
116 a) S. Yoshimoto, N. Higa, K. Itaya, *J. Am. Chem. Soc.* **2004**, *126*, 8540. b) K. Suto, S. Yoshimoto, K. Itaya, *J. Am. Chem. Soc.* **2003**, *125*, 14976.
117 For special issue on Electrochemistry: K. Suto, S. Yoshimoto, K. Itaya, *Langmuir*, accepted.
118 a) M. M. Olmstead, D. A. Costa, K. Maitra, B. C. Noll, S. L. Phillips, P. M. Van Calcar, A. L. Balch, *J. Am. Chem. Soc.* **1999**, *121*, 7090. b) T. Ishii, N. Aizawa, R. Kanehama, M. Yamashita, K.-i. Sugiura, H. Miyasaka, *Coord. Chem. Rev.* **2002**, *226*, 113.
119 S. Yoshimoto, E. Tsutsumi, K. Suto, Y. Honda, K. Itaya, *Chem. Phys.* **2005**, *319*, 147.
120 S. Yoshimoto, E. Tsutsumi, Y. Honda, O. Ito, K. Itaya, *Chem. Lett.* **2004**, *33*, 914.
121 a) S. Yoshimoto, E. Tsutsumi, Y. Honda, Y. Murata, M. Murata, K. Komatsu, O. Ito, K. Itaya, *Angew. Chem., Int. Ed.* **2004**, *43*, 3044. b) S. Yoshimoto, Y. Honda, Y. Murata, M. Murata, K. Komatsu, O. Ito, K. Itaya, *J. Phys. Chem. B* **2005**, *109*, 8547.
122 S. Yoshimoto, A. Saito, E. Tsutsumi, F. D'Souza, O. Ito, K. Itaya, *Langmuir* **2004**, *20*, 11046.
123 a) E. I. Altman, R, J. Colton, *Surf. Sci.* **1992**, *279*, 49. b) E. I. Altman, R. J. Colton, *Surf. Sci.* **1993**, *295*, 13. c) E. I. Altman, R. J. Colton, *Phys. Rev. B* **1993**, *48*, 18244.
124 S. Uemura, A. Ohira, M. Sakata, I. Taniguchi, M. Kunitake, C. Hirayama, *Langmuir* **2001**, *17*, 5.
125 S. Yoshimoto, S. Sugawara, K. Itaya, *Electrochemistry* **2006**, *74*, 175.
126 Y.-B. Wang, Z. Lin, *J. Am. Chem. Soc.* **2003**, *125*, 6072.
127 V. A. Basiuk, *J. Phys. Chem. A* **2005**, *109*, 3704.
128 D. Bonifazi, H. Spillmann, A. Kiebele, M. de Wild, P. Seiler, F. Cheng, T. Jung, F. Diederich, *Angew. Chem., Int. Ed.* **2004**, *43*, 4759.
129 a) S. Yoshimoto, E. Tsutsumi, O. Fujii, R. Narita, K. Itaya, *Chem. Commun.* **2005**, 1188. b) Y. Zhao, Z. Chen, H. Yuan, X. Gao, L. Qu, Z. Chai, G. Xing, S. Yoshimoto, E. Tsutsumi, K. Itaya, *J. Am. Chem. Soc.* **2004**, *126*, 11134.
130 a) K. Komatsu, M. Murata, Y. Murata, *Science* **2005**, *307*, 238. b) K. Komatsu, Y. Murata, *Chem. Lett.* **2005**, *34*, 886.
131 a) F. D'Souza, M. E. Zandler, P. M. Smith, G. R. Deviprasad, K. Arkady, M. Fujitsuka, O. Ito, *J. Phys. Chem. A* **2002**, *106*, 649. b) M. E. Zandler, P. M. Smith, M. Fujitsuka, O. Ito, F. D'Souza, *J. Org. Chem.* **2002**, *67*, 9122. c) M. Fujitsuka, N. Tsuboya, R. Hamasaki, M. Ito, S. Onodera, O. Ito, Y. Yamamoto, *J. Phys. Chem. A* **2003**, *107*, 1452.
132 a) M. Sawamura, Y. Kuninobu, M. Toganoh, Y. Matsuo, M. Yamanaka, E. Nakamura, *J. Am. Chem. Soc.* **2002**, *124*, 9354. b) M. Toganoh, Y. Matsuo, E. Nakamura, *Angew. Chem., Int. Ed.* **2003**, *42*, 3530.
133 J. Y. Zheng, K. Tashiro, Y. Hirabayashi, K. Kinbara, K. Saigo, T. Aida, S. Sakamoto, K. Yamaguchi, *Angew. Chem., Int. Ed.* **2001**, *40*, 1858.
134 S. Yoshimoto, A. Saito, K. Itaya, unpublished results.
135 a) C. A. Hunter, M. N. Mesh, J. K. M. Sanders, *J. Am. Chem. Soc.* **1990**, *112*, 5773. b) H. L. Anderson, C. A. Hunter, M. N. Mesh, J. K. M. Sanders, *J. Am. Chem. Soc.* **1990**, *112*, 5780.
136 L. Baldini, C. A. Hunter, in *Advances in Inorganic Chemistry Including Bioinorganic Studies*, ed. by A. G. Sykes, Academic Press, San Diego, **2002**, Vol. 53, p. 213.
137 a) M. Fujita, K. Umemoto, M. Yoshizawa, N. Fujita, T. Kusukawa, K. Biradha, *Chem. Commun.* **2001**, 509. b) M. Fujita, M. Tominaga, A. Hori, B. Therrien, *Acc. Chem. Res.* **2005**, *38*, 371.
138 A. L. Kieran, A. D. Bond, A. M. Belenguer, J. K. M. Sanders, *Chem. Commun.* **2003**, 2674.
139 X. Peng, N. Aratani, A. Takagi, T. Matsumoto, T. Kawai, I.-W. Hwang, T. K. Ahn, D. Kim, A. Osuka, *J. Am. Chem. Soc.* **2004**, *126*, 4468.
140 O. Shoji, S. Okada, A. Satake, Y. Kobuke, *J. Am. Chem. Soc.* **2005**, *127*, 2201.
141 E. Deiters, V. Bulach, M. W. Hosseini, *Chem. Commun.* **2005**, 3906.
142 P. C. M. van Gerven, J. A. A. W. Elemans, J. W. Gerritsen, S. Speller, R. J. M. Nolte, A. E. Rowan, *Chem. Commun.* **2005**, 3535.

143 a) A. Dmitriev, H. Spillmann, N. Lin, J. V. Barth, K. Kern, *Angew. Chem., Int. Ed.* **2003**, *42*, 2670. b) S. Stepanow, M. Lingenfelder, A. Dmitriev, H. Spillmann, E. Delvigne, N. Lin, X. Deng, C. Cai, J. V. Barth, K. Kern, *Nat. Mater.* **2004**, *3*, 229. c) M. A. Lingenfelder, H. Spillmann, A. Dmitriev, S. Stepanow, N. Lin, J. V. Barth, K. Kern, *Chem. Eur. J.* **2004**, *10*, 1913. d) S. Stepanow, N. Lin, F. Vidal, A. Landa, M. Ruben, J. V. Barth, K. Kern, *Nano Lett.* **2005**, *5*, 901. e) T. Classen, G. Fratesi, G. Costantini, S. Fabris, F. L. Stadler, C. Kim, S. de Gironcoli, S. Baroni, K. Kern, *Angew. Chem., Int. Ed.* **2005**, *44*, 6142.

144 a) M. Abe, T. Michi, A. Sato, T. Kondo, W. Zhou, S. Ye, K. Uosaki, Y. Sasaki, *Angew. Chem., Int. Ed.* **2003**, *42*, 2912. b) M. Abe, T. Masuda, T. Kondo, K. Uosaki, Y. Sasaki, *Angew. Chem., Int. Ed.* **2005**, *44*, 416.

Soichiro Yoshimoto was born in Kumamoto, Japan, in 1973. He received his B.Eng. (1995), M.Eng. (1997), and Ph.D. (2000) from Kumamoto University on the research subject on "Electrochemical and STM Studies on Gold Single Crystal Electrodes Modified with Pyridinethiols" under the supervision of Prof. I. Taniguchi. Then, he joined Prof. K. Itaya's group at Tohoku University from April in 2000 to March in 2005 as a research associate. Since March in 2005, he has been a researcher of the Biosensing Technology Research Group of the National Institute of Advanced Industrial Science and Technology (Tsukuba). He received the Electrochemical Society of Japan Award for Young Electrochemists in 2006. His current interest involves supramolecular surface design using porphyrins, phthalocyanines fullerenes and organothiols for functional and biological interfaces and characterization of such surfaces by electrochemistry and STM.